International Journal of Multiphase Flow 91 (2017) 19–38

Contents lists available at ScienceDirect

International Journal of Multiphase Flow

journal homepage: www.elsevier.com/locate/ijmulflow

A Coupled Level Set and Volume of Fluid method for automotive exterior water management applications

M. Dianat, M. Skarysz, A. Garmory*

Department of Aeronautical and Automotive Engineering, Loughborough University, Loughborough, LE11 3TU, UK

ARTICLE INFO

Article history:
Received 7 June 2016
Revised 11 January 2017
Accepted 23 January 2017
Available online 23 January 2017

Keywords:
Surface flows
Level set
Volume of Fluid
CLSVOF
Contact angle

ABSTRACT

Motivated by the need for practical, high fidelity, simulation of water over surface features of road vehicles a Coupled Level Set Volume of Fluid (CLSVOF) method has been implemented into a general purpose CFD code. It has been implemented such that it can be used with unstructured and non-orthogonal meshes. The interface reconstruction step needed for CLSVOF has been implemented using an iterative 'clipping and capping' algorithm for arbitrary cell shapes and a re-initialisation algorithm suitable for unstructured meshes is also presented. Successful verification tests of interface capturing on orthogonal and tetrahedral meshes are presented. Two macroscopic contact angle models have been implemented and the method is seen to give very good agreement with experimental data for a droplet impinging on a flat plate for both orthogonal and non-orthogonal meshes. Finally the flow of a droplet over a round edged channel is simulated in order to demonstrate the ability of the method developed to simulate surface flows over the sort of curved geometry that makes the use of a non-orthogonal grid desirable.

1. Introduction

There are several engineering applications which involve the flow of liquid droplets or rivulets over solid surfaces. One such application is 'Exterior Water Management' (EWM) on road vehicles. EWM is important when driving, for example managing the water flowing from the windscreen onto the side glass, or stripping off the wing-mirror housing and impacting the side glass and thereby obscuring vision. It is also important in static situations where water run-off from the roof can enter the vehicle, making seats or the luggage space wet. Hence the motion of individual drops under gravity is of interest when designing features such as drainage channels which prevent this. Hagemeier et al. (2011) provides a thorough review of the issue of vehicle EWM and the state of the art of numerical simulation. His review indicates that there are a number of significant gaps in the simulation capability and because the water management features, such as channels, must be fixed at an early stage in the vehicle design it is clear that an accurate method to simulate EWM and contamination would be highly advantageous. Examples of EWM simulations can be found in Gaylard et al. (2012) and Jilesen et al. (2015) that both use Lagrangian particle tracking for the airborne droplets and a 2D film model for the surface flow. While the approach to the dispersed phase (airborne) may be satisfactory, the assumption that the surface flow can be modelled using a 2D film assumption has limitations.

Two dimensional film models such as that used in Gaylard et al. (2012) and Jilesen et al. (2015) or that implemented in OpenFOAM following Meredith et al. (2013) solve transport equations for the film thickness but do not resolve the 3D shape of the surface water. In doing so these models make the assumptions that there is no velocity in the liquid normal to the surface and that the three dimensional shape of the film is not important. While it is possible to use this type of film model to predict the motion of droplets and rivulets there will be situations where these assumptions will not hold. For example droplets filling or crossing a drainage channel will have significant velocities normal to the surface and an example of this is included in Section 6. For the cases where aerodynamic drag on the drop or rivulet is important then the two-way coupling between the forces on the liquid and its shape will be important. A thin film approximation cannot simulate this as it does not change the shape of the boundary seen by the flow solver unless complex mesh morphing techniques are also used.

Fluid film models also make use of empirical sub models to account for phenomena such as droplet impingement or film stripping. For these to give accurate predictions it is necessary to use them for the circumstances they were derived for. For example the film model used in the OpenFOAM fluid film model uses a film stripping model (Owen and Ryley, 1985) which assumes that if the

* Corresponding author.
E-mail address: A.Garmory@lboro.ac.uk (A. Garmory).

http://dx.doi.org/10.1016/j.ijmultiphaseflow.2017.01.008

film is stripped off the surface it breaks down immediately into a spray of droplets small in comparison to the computational mesh. Hence this model would not give correct results in cases where the liquid leaves the surface in a coherent mass.

The focus of this paper is therefore on developing methods that overcome this limitation. There are a number of requirements for a method suitable for the practical simulation of 3D droplets rivulets and films on a vehicle surface:

- It would require both high resolution of the water surface in 3D to capture droplet shapes, particularly at the surface contact line, and mass conservation to simulate droplet motion over large distances.
- It is essential for the method to work with realistic geometry, including highly curved surfaces, such as those found on vehicles.
- Implementation in a general purpose CFD code will make the method a more practical tool for real applications.
- The method must include the different behaviour of water on different surfaces such as paintwork, glass or treated hydrophobic surfaces.

1.1. Interface capturing methods

Several numerical methods have been developed for 3D interface capturing in multiphase Computational Fluid Dynamics (CFD) which may be relevant for EWM simulations. The most common ones are Front Tracking, Volume of Fluid (VOF), Level Set (LS) and Coupled Level Set and VOF (CLSVOF). Front tracking methods, see for example Tryggvason et al. (2001), represent the interface between the phases using a series of points, joined by triangular elements, located on the interface. The location of a CFD cell relative to this interface determines the fluid properties (i.e. those of liquid or gas) which are used to calculate the velocity field. The points defining the interface are then moved in a Lagrangian fashion using velocities interpolated from the CFD velocity field. The method is able to give precise definition for the interface location but does not strictly conserve mass. Marić et al. (2015) have recently implemented a hybrid Level Set/Front Tracking method for unstructured grids and have, so far, presented results for some test cases but not ones including surface flows.

With the VOF method, the volume fraction, α, is defined as the fraction of volume occupied by the liquid in each cell. VOF is thus bounded between 0 and 1 but changes discontinuously across the interface, see Scardovelli and Zaleski (1999) for a review of the approach. The evolution of α is governed by a simple advection equation using the resolved velocity field. The advantage of VOF is that mass is correctly conserved and it can be applied on any mesh. The simplest, and easiest to implement, VOF method is 'algebraic VOF' where the VOF field is transported by a convection term using standard discretisation methods. However, numerical diffusion in the transport scheme causes non-physical smearing of the interface leading to a loss of accuracy in the definition of the interface location. A method of defining or 'reconstructing' the interface location within a cell using the value of α and the normal to the interface given by $\nabla\alpha$ can be used to overcome this. Such methods are classed as 'geometric VOF,' see Scardovelli and Zaleski (1999) or for a recent example Marić et al. (2013). But as the magnitude of $\nabla\alpha$ should ideally be infinite at the interface, this can lead to numerical problems in the evaluation of this and the interface reconstruction.

An alternative choice for interface capturing, proposed by Sussman et al. (1994), is the Level Set (LS) method. Unlike α, LS function, ϕ, is a continuous variable. It is defined as the signed distance from the interface being positive in the liquid and negative in the gas and zero at the interface itself. LS function is also evolved by another simple advection equation using the resolved velocity field. The advantage of LS methods is that they give a sharp definition to the interface but the disadvantage is that they are not mass conservative and therefore require high-order numerical schemes. For example the Level Set approach was applied by Griebel and Klitz (2013) who used a Cartesian mesh with a 5th order WENO scheme to simulate the motion of a droplet impinging on a plate. More recently a conservative form of the Level Set approach has been developed by Pringuey and Cant (2014) for use with unstructured meshes. Early results with this method are encouraging but the method still relies on high order spatial schemes which are complex to implement particularly in general purpose unstructured CFD codes.

Previous researchers have combined the advantages of LS and VOF methods. Albadawi et al. (2013) proposed a simple coupled Level Set Volume of Fluid (S-CLSVOF) which was also later used by Yamamoto et al. (2016). In this method a transport equation is solved for VOF but not the Level Set. Instead a Level Set is constructed from the interface (defined as the VOF = 0.5 isosurface). This allows more accurate calculation of the surface curvature using the level set.

A fully Coupled LS/VOF (CLSVOF) method was proposed by Sussman and Puckett (2000) and has been implemented by a number of researchers, e.g. Menard et al (2007) and Wang et al. (2009). In this fully coupled method transport equations are solved for both a level-set field and a VOF field. These are used together to reconstruct the interface within a cell. The level set provides a defined contour for the interface and a smoothly differentiable field while the VOF ensures mass conservation even on coarse meshes. Details of the CLSVOF method implemented in an in-house code for structured grids with no contact models can be found in Xiao (2012), and Xiao et al. (2013, 2014a,b). Yokoi (2013) applied the method using a Cartesian structured grid to the problem of droplet splashing, showing the method's suitability for EWM type applications. Previously the CLSVOF method has been applied using orthogonal meshes. An interesting recent development was published by Arienti and Sussman (2014) in which they use a Cartesian adaptive grid with the CLSVOF method but include complex surface geometry by defining it as a second level-set function on the Cartesian grid. In this paper we present a method based on the Coupled Level-Set Volume of Fluid (CLSVOF) implemented such that it can be used in non-orthogonal or unstructured meshes. However in order for it to be used for EWM applications it will also need to include some method of modelling surface contact properties.

1.2. Surface contact modelling

With the surface contamination application, interaction between the liquid, gas and solid surface introduces additional complexity. The surface water flow will be affected by the different surfaces it flows over, for example automotive paintwork, glass, seals and possibly specially treated hydrophobic surfaces. Sui et al. (2014) provides a thorough review of the topic of the moving contact line problem. The motion of the contact line across the surface implies a contradiction with the no-slip boundary condition used in viscous flow CFD. This apparent contradiction must be resolved by the use of some physical modelling to include the effect of this singularity. A widely used method is to allow for a 'slip length' at the contact point, see for example Dussan (1979). As discussed by Sui et al. (2014) to fully capture all the physics involved requires resolving a very wide range of scales. To do this in a CFD calculation would require a very high mesh resolution, much higher even than that typically required for a DNS calculation of turbulent flow. For practical situations this will be prohibitively expensive.

The alternative is to use the approach of specifying a macroscopic contact angle. In this approach the 'apparent' contact angle observed at the scale of the mesh resolution is applied as a boundary condition with the implicit assumption that there is a slip length smaller than the near wall CFD cell. This 'sub-grid' modelling of the contact angle was employed with a VOF method in Dupont and Legendre (2010) and Legendre and Maglio (2013). They were able to successfully validate this approach for the simulation of static and sliding contact lines. Afkhami et al. (2009) developed a macroscopic contact angle boundary condition which takes into account the size of the near wall cell and were able to produce results with good mesh convergence in a VOF calculation.

This approach allows the inclusion of surface properties in the calculation by making the macroscopic contact angle a function of the surface and liquid properties as well as the contact line velocity. This approach has been applied in several previous studies. Yokoi et al. (2009) presented results obtained with a CLSVOF method using a 2D uniform Cartesian mesh. They are able to show that with the correct contact angle specified very good agreement with experiment can be obtained. Griebel and Klitz (2013) have also simulated the same experiment using a Level Set method with a uniform grid and high-order numerical schemes. They test the contact angle model given by Yokoi et al. (2009) along with an alternative model suggested by Shikhmurzaev (2008). These works show if the contact angle model is specified correctly then the correct droplet dynamics can be reproduced using this macroscopic approach. This is the method that will be applied in this paper. Two contact angle models have been used in this paper and details of them can be found in Section 3.

1.3. Objectives and structure of paper

The objective of this work is to develop an interface capturing CFD method suitable for simulating the motion of water over the surface of road vehicles. The method uses a CLSVOF technique to ensure precise interface definition and mass conservation. In order for the method to be used for realistic curved geometry it has been implemented into the general purpose open source solver OpenFOAM (OpenFOAM, 2013) using a formulation suitable for non-orthogonal grids. The method will use a macroscopic contact angle modelling approach to include surface contact physics into the simulations. The method, which is built on an existing VOF solver, is presented in Section 2 and the contact angle models used are in Section 3. Several verification tests of the CLSVOF interface capturing for unstructured grids in two and three dimensions are presented in Section 4. The full method, including momentum solver, is validated against experimental data for a droplet impinging on a plate in Section 5 before the capability of the solver to simulate a droplet flowing across curved surfaces is demonstrated for a generic channel overflow case in Section 6.

2. Implementation of a CLSVOF method for unstructured grids

The Coupled Level-Set Volume of Fluid interface capturing method presented in this paper has been implemented as an extension to the existing 'interFoam' algebraic VOF solver available in OpenFOAM. The new developments are intended to lead to an accurate multiphase approach using unstructured grids suitable for simulating exterior surface water flow on road vehicles. As the starting point of the current work, the existing algebraic VOF implementation within OpenFOAM is briefly outlined in Section 2.1. Section 2.2 describes the algorithm for the interface capturing methodology implemented as part of the CLSVOF formulation. The method involves reconstruction of the interface position within interface cells based on an iterative procedure using the LS gradient and local VOF value. This is described in Section 2.2.1, including the procedure for calculating the volume of the arbitrary shape formed when the interface plane intersects a cell. The re-initialisation method for unstructured grids is intended to ensure that the Level-Set remains a signed distance function; the procedure is presented in Section 2.2.2.

Although the flow for the test cases considered in Sections 5 and 6 are laminar, the solution approaches outlined in the following sections can be extended to include turbulent flow either in RANS or LES or even DNS form. For such cases, the current procedure for interface capturing will remain unchanged but solution of the Navier-Stokes equations must include turbulence related terms such as subgrid-scale turbulence and suitable inlet conditions for the LES.

2.1. Algebraic VOF solver (interFoam)

The standard OpenFOAM code (version 2.1.1) has an algebraic VOF solver 'interFoam' implemented (OpenFOAM, 2013). This has been used as the basis for the CLSVOF code. Results with the interFoam solver have also been obtained for comparison with CLSVOF and some details of the interFoam solver are presented here for reference. Further details can be found in Weller (2008), Desphande et al (2012) and Márquez Damián (2013). It uses an algebraic VOF algorithm where an advection equation for the liquid volume fraction, α, is solved

$$\frac{\partial \alpha}{\partial t} + \nabla .\ (U\alpha) = 0 \tag{1}$$

This equation is solved using an explicit temporal solver with a first or second order spatial discretisation scheme. For the interFoam calculations presented in this work, first order Euler method for temporal and limited van Leer (1974) TVD scheme for spatial discretisation were used which yield bounded α between 0 and 1.

The velocity field is then found by solving the momentum and pressure equations using the OpenFOAM pressure-velocity PIMPLE correction procedure. The PIMPLE algorithm is the merged PISO-SIMPLE predictor-corrector solver for large time step transient incompressible laminar or turbulent flows. It is based on an iterative procedure for solving equations for velocity and pressure. PISO (Pressure Implicit Split Operator) is a transient solver and SIMPLE (Semi Implicit Method for Pressure Linked Equations) is a steady-state solver for incompressible flows. A single set of momentum equations are solved for both phases. For incompressible isothermal flow the momentum equation is

$$\frac{\partial (\rho U)}{\partial t} + \nabla .(\rho UU) = -\nabla p + \nabla .\ \tau + \rho g + f_\sigma \tag{2}$$

Here, U is velocity, p is pressure, τ is viscous stress, g is gravitational acceleration and f_σ represents the surface tension force. The viscous stress is obtained from the velocity tensor assuming Newtonian fluids. The density and viscosity needed in the momentum equation are calculated from

$$\rho = \alpha \rho_L + (1-\alpha)\rho_G \tag{3}$$

$$\mu = \alpha \mu_L + (1-\alpha)\mu_G \tag{4}$$

This ensures that the correct liquid and gas properties will be used away from the interface, while for interface cells the mean momentum of the contents of the cell are solved using volume averaged transport properties. The surface tension effect in the momentum equations is based on the Continuum Surface Force (CSF) (Brackbill et al. 1992) with $f_\sigma = \sigma \kappa\ \nabla \alpha$ where σ is the surface tension coefficient of liquid in gas and κ is the mean curvature of the free surface obtained from

$$\kappa = -\nabla .\ \frac{\nabla \alpha}{|\nabla \alpha|} \tag{5}$$

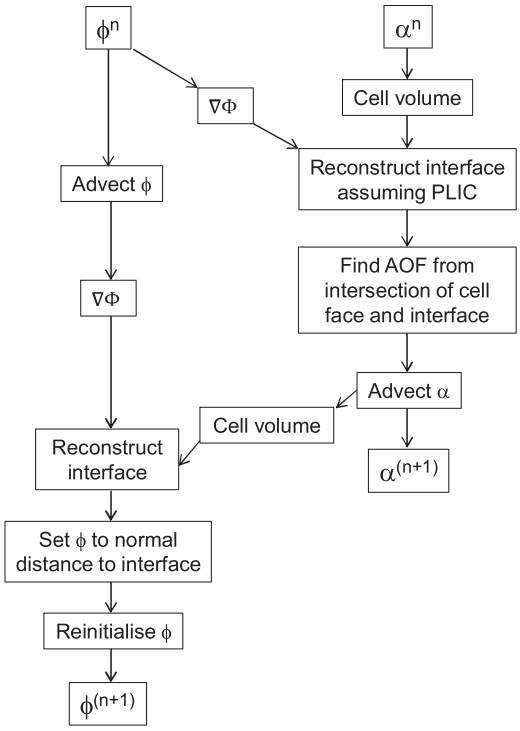

Fig. 1. Overview of interface capturing algorithm used to update VOF, α, and Level Set, ϕ.

Here $\nabla\alpha$is calculated using a linear Gauss method available in OpenFOAM.

As with any transport equation the VOF solution will contain some numerical diffusion due to discretisation error. To counter this, the interFoam solver also includes the addition of an optional compression velocity to sharpen the interface. With this addition, the VOF advection equation takes the following form

$$\frac{\partial\alpha}{\partial t} + \nabla.\,(U\alpha) + \nabla.\,[U_r\alpha(1-\alpha)] = 0 \tag{6}$$

where $U = \alpha U_L + (1-\alpha)\,U_G$ is the weighted average velocity and $U_r = U_L - U_G$ is the relative velocity vector between liquid and gas designated as the '*interface compression velocity*' in OpenFOAM calculated from

$$U_r = \min\left(c_\alpha \frac{|\chi|}{|S_f|}, \max\left(\frac{|\chi|}{|S_f|}\right)\right) n_f \tag{7}$$

Here, χ is face volume flux, S_f is the face normal vector, n_f is the face unit normal flux and c_α is a scalar parameter controlling the extent of artificial compression velocity usually between 0 and 2 with the recommended value of 1. Later versions of OpenFOAM include additions to interFoam to include a Crank Nicholson temporal scheme and an optional isotropic compression velocity. However these have not been used here to enable comparison with the method discussed in the published works of Weller (2008), Desphande et al (2012) and Márquez Damián (2013).

2.2. Coupled Level Set VOF (CLSVOF)

In the following sections, our new CLSVOF model incorporated in OpenFOAM will be described. This implementation is designed to provide accurate interface capture on both structured and unstructured grids together with the existing functionality of the OpenFOAM multiphase solver. A flow chart summarising the interface capturing algorithm is shown in Fig. 1.

The solution domain is first initialised with the initial VOF and LS fields. The interface is then reconstructed from LS and VOF fields. The value of VOF in the interface cells gives the volume on each side of the interface while the gradient of the LS field at the interface gives the direction normal to the interface. These pieces of information, together with a Piecewise-Linear Interface Calculation (PLIC) approximation of the interface, are sufficient to enable the calculation of the position of the interface. The method employed to do this is described in detail in Section 2.2.1. With the position of the interface known, its intersection with the cell faces can also be found. In this way the fraction of each face occupied by liquid can be found from the intersection of the face and the interface to define a face 'Area of Fluid' (AOF).

These AOF values, are then used in the VOF advection process. The volume flux from one cell to its neighbour is found by multiplying the local velocity by the AOF value for that face found by reconstructing the interface in the upwind cell.

$$\frac{\partial\alpha}{\partial t} = -\frac{1}{V}\sum_i AOF_i \boldsymbol{U_i}\cdot\boldsymbol{S_{fi}} \tag{8}$$

Where V is the volume of the cell and the summation is over all faces of the cell. The value of AOF away from the interface will be equal to 0 or 1. For parallel calculation at processor-processor interfaces this information must be communicated between processors. By using the reconstructed AOF value in this way the CLSVOF method ensures that liquid can only be transported from a cell to its neighbour if the interface intersects the face connecting those cells. The face fluxes found from the reconstruction process are stored at this point for use in the momentum solver.

As the fluxes are calculated using values of AOF from the reconstruction step an explicit temporal scheme is used for VOF. The MULES (Multidimensional Universal Limiter with Explicit Solution) explicit solver available in OpenFOAM is used for temporal integration. Details of this can be found in Márquez Damián (2013) but essentially the fluxes into or out of a cell are limited if VOF would become unbounded. In practice we use this by supplying the volume flux from the AOF as the 'high-order' flux to the MULES solver. The use of the limiter in this way will maintain boundedness and stability of the full code as time steps become bigger at the expense of some reduction in accuracy. The time step can be set either as a constant or using the variable time step option in OpenFOAM. The latter is based on a CFL criterion which can be specified globally as

$$CFL_G = \left(\frac{\sum|\phi_f|}{V}\right)_{max}\Delta t \tag{9}$$

(where ϕ_f is the face flux found from the velocity field) or only using cells at the interface, CFL_α by filtering by VOF value using $\alpha(1-\alpha)$. The time step is then adjusted using target global and interface CFL numbers according to

$$\Delta t_{new} = \min\left(\frac{CFL_{G,target}}{CFL_G}, \frac{CFL_{\alpha,target}}{CFL_\alpha}\right)\Delta t_{old} \tag{10}$$

The choice of time step or CFL number is given for each test case in the relevant section.

The LS field is also advected using the following equation

$$\frac{\partial\phi}{\partial t} + \nabla.\,(U\phi) = 0 \tag{11}$$

LS equation is solved using a van Leer TVD spatial scheme. Once the VOF and LS fields have been updated the reconstruction step can be repeated to find the new interface location using the method presented in Section 2.2.1. During this second reconstruction step the Level Set within those cells including an interface is then made equal to the distance between the cell centre and the

interface plane, with positive sign if the cell centre is inside the liquid or negative otherwise. This ensures that the LS = 0 isosurface remains consistent with the reconstructed interface.

It is well known that ϕ fails to remain a distance function as the computations are progressed. Therefore a re-initialisation step is applied to ensure that $|\nabla\phi| = 1$. This is done following the method described in Sussman et al. (1994) adapted for unstructured grids. Further detail of this is given in Section 2.2.2. After solving the re-initialisation equation, the interface capturing process for the current time step is completed. As the step begins with the interface reconstruction process this means that the LS gradient used to define the interface for the advection step is consistent with the LS field after it has been corrected by the re-initialisation step.

The momentum and pressure equations are now solved using the same pressure-velocity correction procedure as outlined in Section 2.1; however the mass flux used in the momentum transport term is now found from the stored AOF values from the reconstruction process. As with the original VOF solver the local density and viscosity are determined using volume weighted averages found from the VOF field.

With this approach, the physical properties used in the momentum equations are treated as weighted averages in the vicinity of the interface based on the volume fraction field. Elsewhere, the properties represent the actual liquid or gas properties. Such approximation contradicts the immiscibility assumption of two fluids near the interface but can be thought of as providing volume averaged properties suitable for calculating the volume averaged momentum in the cell. This leads to stable solutions for high liquid to gas density ratio test cases, as employed here, without requiring an extrapolated liquid velocity field for the gas phase near the interface, together with the imposition of divergence free step for that, as is the case for example in Sussman et al. (2007). It should be noted that it is not unusual to apply smoothed Heaviside function for LS with some CLSVOF methods that use LS rather than VOF to obtain physical properties, see e.g. Sussman et al. (1994). These also violate the immiscibility assumption of gas and liquid in order to provide more stable numerical solutions. Linear interpolations based on the LS are also frequently performed to derive cell face values for the physical properties leading to values that are different from the actual ones, see e.g. Sussman et al (2000). Our choice of the current method is based on a compromise between simplicity, stability and accuracy. It is also consistent with the existing VOF formulation within OpenFOAM thus requiring minimal change to the structure of the solver.

Similarly, to maintain consistency with the momentum and pressure implementation in the existing interFoam solver, the surface tension is again found with the CSF method, $f_\sigma = \sigma\kappa\ \nabla\alpha$, where σ is the surface tension coefficient of liquid in gas and κ is the mean curvature of the free surface. Using the gradient of the VOF field here ensures that the surface tension is local to the interface. An alternative is to use either a suitable approximation to a delta function on Level-set or the gradient of the Heaviside function of the Level-set as discussed in Yamamoto et al. (2016). Both approached would require some smoothing of either the delta function or the gradient of the Heaviside function, and hence a further modelling choice. For the implementation here the gradient of the smoothed Heaviside function, $\nabla(H(\phi))$, is likely to be strongly related to $\nabla\alpha$. In practice, preliminary testing of the use of $\nabla(H(\phi))$ and $\nabla\alpha$ gave very similar results. However, unlike the existing interFoam solver, with the CLSVOF method the curvature term is obtained from

$$\kappa = -\nabla.\ \frac{\nabla\phi}{|\nabla\phi|} \tag{12}$$

Note that contrary to the pure VOF method where curvature is obtained from the VOF, it is now a function of the Level Set. This should lead to a more accurate estimate of the surface tension force which always plays an important role in any two-phase flow. This method is seen to work well for the test case employed in this work for which stable operation is seen and accurate results observed.

The solution at this level provides the new interface and velocity fields to be used at the next time step. As no higher order numerical schemes are required than are used in the standard OpenFOAM VOF implementation, there is no extra implementation required for parallel operation other than to communicate face AOF values and LS face gradients needed in the LS re-initialisation routine. The key step in the CLSVOF method for arbitrary grids is the calculation of the AOF value on cell faces using reconstruction of the interface position; this is discussed in the next section.

2.2.1. Geometrical algorithm for interface reconstruction

The interface location and its intersection with cell faces needs to be established based on an approximation to the interface, the cell volume fraction and the interface normal provided by the gradient of the level set field. Each cell with $0 < \alpha < 1$ must involve an interface. The most common interface representation consists of a plane and this class of interface representation is termed as Piecewise-Linear Interface Calculation (PLIC). The interface gradient vector (i.e. the vector normal to the surface) and any point on the interface will be sufficient to define exactly the interface location. The intercept of this interface with the cell faces can then be determined to find an exact AOF value on these faces.

When the CLSVOF method is employed on an orthogonal rectangular mesh, the interface location can be established analytically by solving an equation based on the known geometry of the cell. See for example Xiao et al (2014a,b) for details of how this can be achieved.

However the procedure for establishing the position of the interface plane within the cell is more complicated on arbitrary meshes. Here we apply an iterative method where the plane interface is shifted in the direction of the surface normal until the volume occupied by the shape bounded by the cell and the interface matches the cell volume fraction. A similar method is presented by Marić et al. (2013) who employ a geometric VOF formulation in which the interface is reconstructed using the VOF solution alone by using the cell α and $\nabla\alpha$. With geometric VOF the gradient of volume fraction is defined only in the immediate vicinity of the interface and some smoothing is usually essential to enhance numerical stability which further affects the accuracy of the VOF solution itself (see Marić et al. (2013)). With the CLSVOF approach, on the other hand, the interface gradient is calculated from the level set field. As level set is continuous, it provides a reliable estimate of the interface gradient.

Here we follow the methods for geometrical interface reconstruction developed in Ahn and Shashkov (2008) which were subsequently used by Marić et al. (2013). The reader is referred to these works for detailed explanation and discussion of this works but the basic method is described here for convenience. The method starts by identifying the cell vertices which constitute the extreme possible locations of the interface based on its normal direction. This provides the space in which the iterative algorithm must look for the location of the interface. At each iteration it is necessary to find the volume of the part of the cell bounded by the interface position for the current iteration. This is not straightforward on an arbitrary grid as the number of faces and edges, as well as their angles to each other, is not known in advance. These numbers can also change during the iterative process as the interface is moved from one side of the cell to the other. The approach used here is based on the clipping and capping algorithm proposed

by Ahn and Shashkov (2008). In this method intersected faces are 'clipped' by the interface to form liquid polygons on the faces (at the final iteration these can be used to find the AOF values). These are then 'capped' by the interface polygon which joins these to form a liquid polyhedron whose volume can be found. This volume can be compared to the known volume provided by the VOF value for the cell and an iterative algorithm used to shift the interface until the volume matches the target to within some specified tolerance. The tolerance used in this work for the interface reconstruction was based

$$\frac{|VOF_{target} - VOF|}{VOF_{target}} < 0.001 \tag{13}$$

In Marić et al. (2013) they follow Ahn and Shashkov by using an iterative algorithm that uses a secant method initially but which switches to a bisection method if the secant fails to converge. As this work represents our first development of a CLSVOF method in OpenFOAM we have used only the bisection algorithm in order to guarantee convergence in all cases. We acknowledge that this incurs a potentially significant time penalty compared to faster iteration methods and this is a clear area for future improvement of our method. Another area of future improvement could be to use the methods such as those developed in López and Hernández (2008) or Diot and François (2016) to define the interface position in arbitrary cells using analytical methods. These methods require several more geometrical operations in the interface cells but could reduce the overall cost compared to iterative methods. However we note that for the impacting drop cases in Section 5 the time penalty of switching from VOF to CLSVOF for the same grid is relatively small.

2.2.2. Re-initialisation of level-set on unstructured meshes

In order to maintain the property that the Level-Set is a signed distance function it is necessary to apply a re-initialisation routine. The re-initialisation equation introduced by Sussman et al. (1994) can be solved every time step to ensure the Level-Set remains a distance function in the vicinity of the interface

$$\frac{\partial \psi}{\partial \tau} = S(\psi_0)\ (1 - |\nabla \psi|) \tag{14}$$

The initial condition is $\psi_0 = \psi(x, \tau = 0) = \phi(x, t)$ and

$$S(\psi_0) = \frac{\psi_0}{\sqrt{\psi_0^2 + (\ |\nabla \psi_0|\ \Delta)^2}} \tag{15}$$

is a modified sign function with $\Delta = \max(\Delta x, \Delta y, \Delta z)$. The re-initialisation equation is solved explicitly in pseudo-time using a fictitious time step. The resulting field is used to update the Level-Set field. At each iteration, it is required to calculate the current gradient magnitude. In order that the correct distance function should propagate away from the interface location (which should be assumed to be fixed in space) the calculation of the gradient for a cell should be found using information from the side of the cell closest to the interface. This can be thought of as being analogous to upwinding for convection. Here we follow the first order scheme described in Sussman et al. (1994) for structured meshes adapted to unstructured meshes. The gradient magnitude is found from

$$|\nabla \psi| = \sqrt{max\left(a_i^2\right) + max\left(b_i^2\right) + max\left(c_i^2\right)} \tag{16}$$

where the subscript i indicates that the max operator is over all faces for the cell. a_i is calculated from the component of the surface normal gradient in the x-direction for face i. The face surface normal gradient, $\frac{\partial \psi}{\partial n}$, is calculated using an explicit non-orthogonal correction available in OpenFOAM. If the face unit normal is $\mathbf{n}$ (directed out of the cell) then the component of the face gradient in the x-direction is $\frac{\partial \psi}{\partial n}\boldsymbol{n} \cdot \boldsymbol{i}$. If the position of the face centre relative to the cell centre is given by the vector $\mathbf{r}$ then a_i is given by

$$a_i = \min\left(0, \frac{\partial \psi}{\partial n}\boldsymbol{n} \cdot \boldsymbol{i}\right), \quad \text{if } (\psi > 0 \ \&\& \ \boldsymbol{r} \cdot \boldsymbol{i} > 0) \ ||\ (\psi < 0 \ \&\& \ \boldsymbol{r} \cdot \boldsymbol{i} < 0) \tag{17}$$

$$a_i = \max\left(0, \frac{\partial \psi}{\partial n}\boldsymbol{n} \cdot \boldsymbol{i}\right), \quad \text{if } (\psi > 0 \ \&\& \ \boldsymbol{r} \cdot \boldsymbol{i} < 0) \ ||\ (\psi \langle 0 \ \&\& \ \boldsymbol{r} \cdot \boldsymbol{i} \rangle 0) \tag{18}$$

The terms b_i and c_i are found from the y and z-components of surface normal gradients in the same way. Processor-processor interface faces are included so that the method works in parallel operation. It is not necessary to include other boundary faces as these will always be located away from the interface other than at the contact point where the contact angle boundary condition will be enforced as described in the next section.

In practical applications a choice of pseudo-time step and number of iterations must be chosen to combine accurate re-initialisation with low cost and stability. For the interface capturing problems presented in this work a pseudo-time step of $\tau = 0.3 \times \min(\Delta x, \Delta y, \Delta z)$ is used together with three iterations for each global time step. The performance of this method in creating a signed distance function from an initially distorted 3D Level-Set field is demonstrated in Section 4.1.

3. Contact angle models for surface flows

A method whereby the macroscopic contact angle is specified as a wall boundary condition is adopted here, rather than attempting to predict the contact angle as part of the simulation. The work of Afkhami et al. (2009) and Legendre and Maglio (2013) showed that it is important to use a near wall grid spacing that is consistent with the macroscopic contact angle definition. Therefore care must be taken about the mesh used as well as the contact angle model. To implement the contact angle model into the CLSVOF formulation we follow the method already available for a generic contact angle model for the interFoam VOF solver in OpenFOAM. This is done by setting the value of LS and VOF for the wall face of an interface cell such that their surface normal gradients are equal to the cosine of the desired contact angle. To do this the dynamic contact angle must first be calculated. This is most often done using a function of Capillary number, $Ca = U_{CL}\mu_L/\sigma$. The contact line velocity used in the calculation of Ca is calculated as the component of the velocity parallel to the wall and normal to the interface, which is positive from liquid to gas and negative otherwise. A wide range of models have been proposed for the dynamic contact angle. The investigation of the available models is beyond the scope of the current work and can be found in many publications (e.g. Puthenveettil et al. 2013, Šikalo et al. 2005). We have used two models which are briefly described below.

3.1. Cox–Voinov model

One of the simplest and commonly used models is the cubic Cox–Voinov model, (Cox 1998 , Voinov 1976), which obtains θ_d from

$$\theta_d^3 - \theta_s^3 = kCa \tag{19}$$

where k is a model parameter given by Hoffman (1975) to be around 72. The static contact angle, θ_s, must be specified for a particular combination of liquid and surface. This parameter, however, is suitable for small capillary flows and could vary significantly depending on the test case examined. It is used here as an example

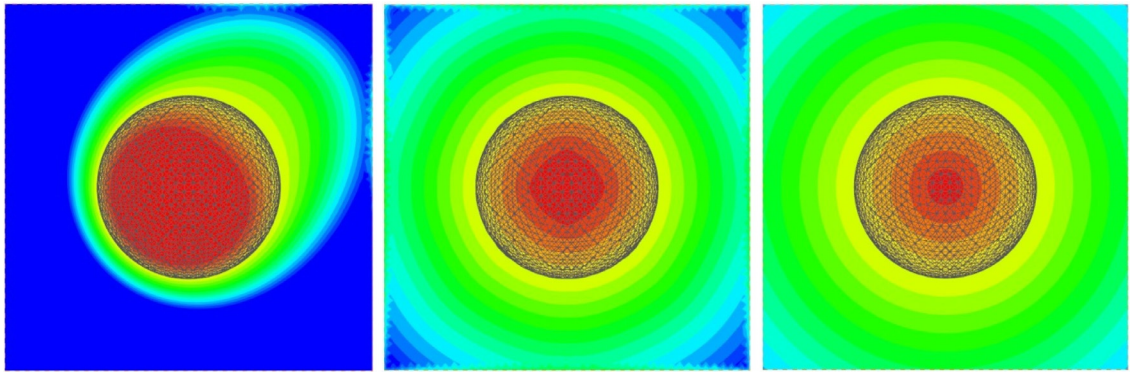

Fig. 2. Contours of: left, initial LS field; middle, LS field after 500 iterations; right, signed distance LS field. Mesh represents the interface.

of a model that is simple to implement and apply to a new problem.

3.2. Yokoi et al. model

The model due to Yokoi et al. (2009) is based on their observation that following the liquid motion, the advancing contact angle continues to increase levelling off ultimately to a maximum value termed as '*maximum dynamic advancing*' angle at high Capillary numbers. Similarly, the receding contact angle continues to decrease reaching to '*minimum dynamic receding*' angle. With Yokoi model, dynamic contact angle is calculated using the curve fitted to the experimental data. This model (Eq. (20)) is based on Tanner's law, Tanner (1979), for Capillary dominated situation (low Ca) and uses constant maximum and minimum angles when inertia is dominant (high Ca).

$$\theta_d = \begin{cases} \min\left[\theta_S + \left(\frac{Ca}{k_a}\right)^{1/3}, \theta_{mda}\right] if\ U_{CL} \geq 0 \\ \max\left[\theta_S + \left(\frac{Ca}{k_r}\right)^{1/3}, \theta_{mdr}\right] if\ U_{CL} < 0 \end{cases} \tag{20}$$

where k_a and k_r are the model parameters and they are chosen to fit the measured contact angles as closely as possible. This model is selected as it is proposed by Yokoi et al and has been derived from their own data. The model is therefore tuned to the data and thus represents a convenient verification test for our CLSVOF implementation.

4. CLSVOF implementation verification test cases

Having described the implementation used in this work we now present a series of verification tests to demonstrate its operation. We first present a test of the ability of the re-initialisation routine to return a distorted LS field to be a signed distance function. We then show interface capturing for prescribed vortex cases in both two and three dimensions.

4.1. Level-set re-initialisation on 3D unstructured mesh

To verify the implementation of the re-initialisation method, the test case described in Min (2010) was used. With this test case, distorted Level-Set field is initialised in a computational domain of $[-2, 2]^3$ as

$$\phi^0(x,y,z) = \left[(x-1)^2 + (y-1)^2 + (z-1)^2 + 0.1\right] \times \left(\sqrt{x^2+y^2+z^2} - 1\right). \tag{21}$$

It defines the interface, i.e. LS = 0 iso-surface, as a sphere of radius 1 with its centre at the origin. However, LS elsewhere is not a signed distance function and its gradients vary significantly as shown in Fig. 2. The re-initialisation routine should converge toward the signed distance field while leaving the location of the interface unchanged.

A 3D unstructured tetrahedral mesh of approximately 930 K elements was used for this purpose. The re-initialisation routine is applied using 250 iterations with a fictitious time step of $\tau = 0.1 \times \min(\Delta x, \Delta y, \Delta z)$ for this tetra mesh. Fig. 2 shows contours of the initial and final level set fields, together with the field representing the exact signed distance function. It can be seen that the re-initialisation routine has caused the initially distorted field to converge towards the exact distribution in the vicinity of the interface on the tetrahedral mesh. Further away from the interface differences can be seen, but for the CLSVOF method it is the field close to the interface which is important. Also shown is the location of the LS = 0 surface which is seen to be correctly left unchanged. Confirmation of the ability of the re-initialisation routine to converge towards the correct signed distance function, without distorting the initial surface position, is shown in Fig. 3.This shows results along a line passing through the centre of the sphere shown in Fig. 2 after 50 and 500 iterations. Note that in the full CLSVOF method the re-initialisation algorithm is applied every timestep so such extreme distortions as seen in Figs. 2 and 3 will not develop. It has been found that three iterations per timestep give satisfactory results.

The test was repeated on a coarser mesh on which the grid spacing was doubled. The error in level set, compared to the exact distance field, averaged over the whole domain is shown against number of iterations in Fig. 4 for both meshes. As expected, due to the use of a fictitious time step chosen to be proportional to the grid space, the global error reduces to a given level in half the number of iterations when the grid spacing is doubled. The corrected field will travel a fixed number of cells per iteration. For the calculation of normal and curvature it is the level set within a certain number of cells of the interface that is important. Therefore Fig. 4 shows that the number of iterations of reinitialisation needed should not need to change with grid spacing.

4.2. Interface capturing test case 1: 2D vortex in a box

The stretching of a liquid disc in a prescribed single vortex flow field is a standard test case to assess the accuracy of interface capturing methods (see Ménard et al. 2007). The test is particularly challenging to interface resolving methods when the resulting liquid ligament becomes thin relative to the grid size. It is used here to evaluate the current CLSVOF method and compare it against the OpenFOAM standard interFoam results. A liquid disc of radius r = 0.15 unit is initially placed at (0.5, 0.75) inside a square box of unit size. The following fixed velocity field is specified as

$$u = \sin(2\pi y) * \sin^2(\pi x) \tag{22}$$

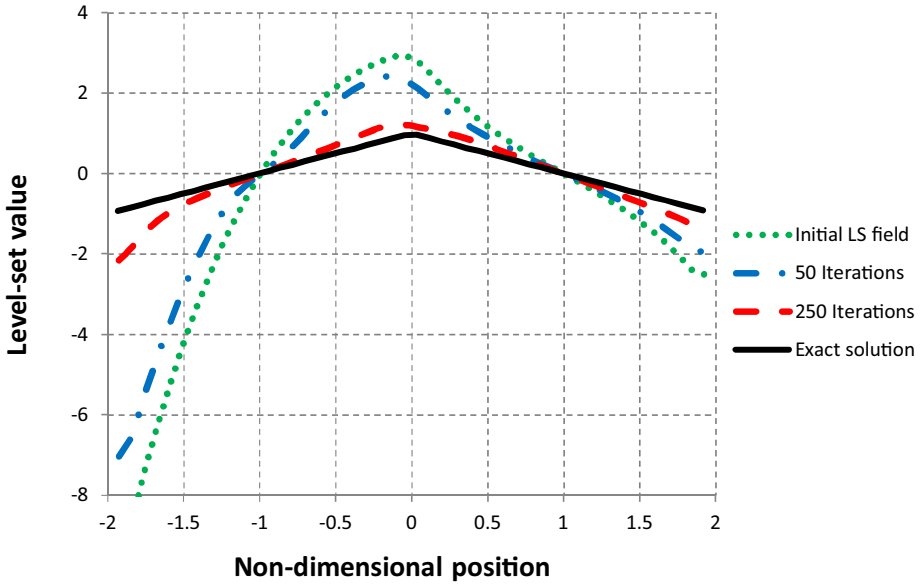

Fig. 3. Level set value along horizontal centre line in Fig. 2. Exact, signed distance is shown, together with initial distorted level-set field and those found after 50 and 250 iterations of the re-initialisation algorithm.

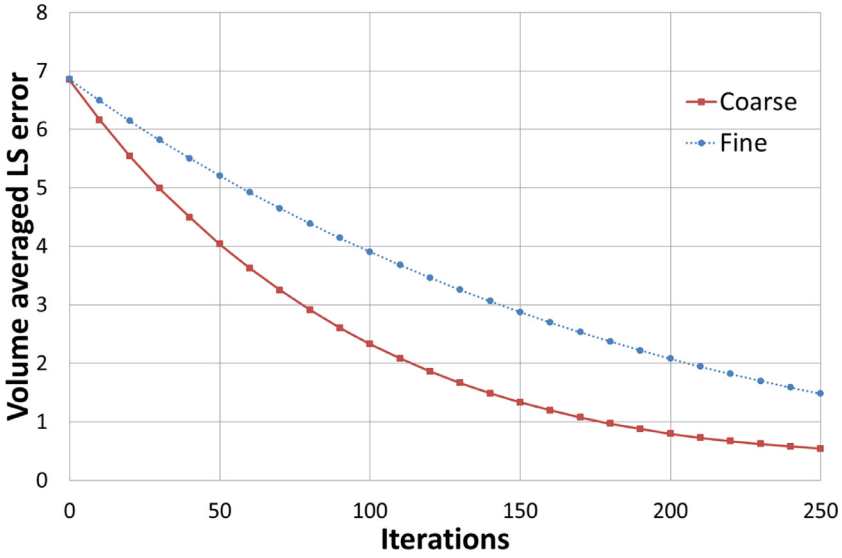

Fig. 4. Volume averaged Level-set error as a function of number of iterations of reinitialisation algorithm on coarse and fine meshes.

$$v = -\sin(2\pi x) * \sin^2(\pi y) \tag{23}$$

and held constant for a period of $T=3$. The velocity field is then reversed for the same period of time which should lead to the recovery of the original VOF and LS fields. The difference between the starting and final states can be used to quantify the error in the solution.

Uniform square meshes of 64^2, 128^2, 256^2 and 512^2 cells were used for the computation of this case with fixed time steps chosen to give the same Courant number in each case of 0.03. This was repeated for three solvers; the interFoam solver with no compression velocity ($c_\alpha = 0$), interFoam with compression ($c_\alpha = 1$) and the CLSVOF method presented in this paper. The volume averaged error in the final VOF field is calculated for each mesh as

$$E_\alpha = \frac{\sum^{V_i} |\alpha_i - \alpha_{i.exact}|}{\sum^{V_i} \alpha_{i.exact}} \tag{24}$$

Where the summation is over all cells *i*. The results are shown in Fig. 5. It can be seen that for all mesh resolutions the CLSVOF algorithm provides an increase in accuracy over the standard VOF method. The CLSVOF method also shows a higher order of convergence than either of the VOF cases. Results for the finest mesh in each case are shown in Fig. 6. The position of maximum stretch is shown as well as the comparison of initial and final interface positions. For the interFoam simulations the final position is shown by the $\alpha = 0.5$ isosurface. One of the drawbacks of algebraic VOF methods, such as interFoam, is that a choice of interface VOF value has to be made which is somewhat arbitrary. CLSVOF on the other hand can use the LS = 0 isosurface as a definitive indicator of the interface location and this is what is shown in the figure.

The test was repeated using meshes of roughly triangular elements with equivalent number of cells to the square case above (so that the typical grid spacing halves each time. The volume averaged VOF error is again plotted against cell number for the three solvers in Fig. 7. It can be seen that while errors are increased

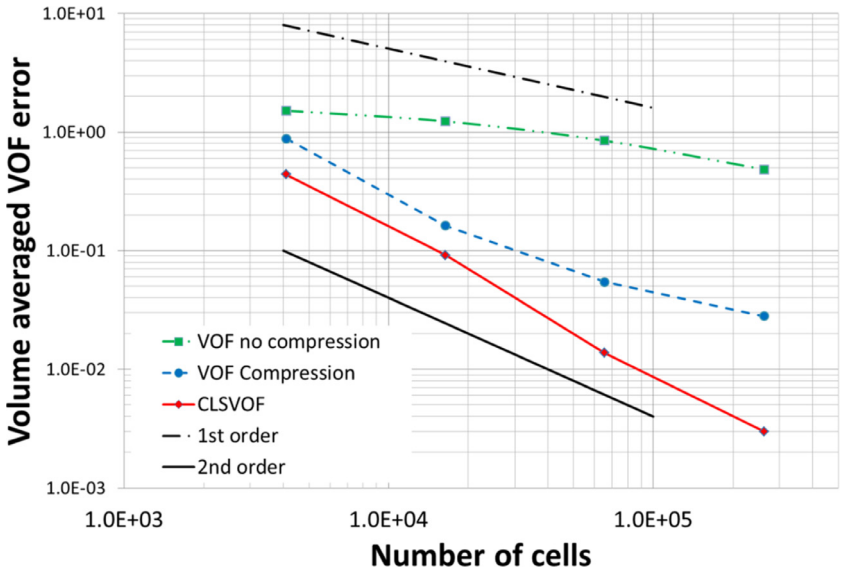

Fig. 5. Volume averaged error of predicted final VOF field for 2D vortex test on successively refined square meshes. Results are shown with standard interFoam algebraic VOF solver with and without compression as well as CLSVOF. Also shown are lines to indicate the gradient given by first and second order convergence.

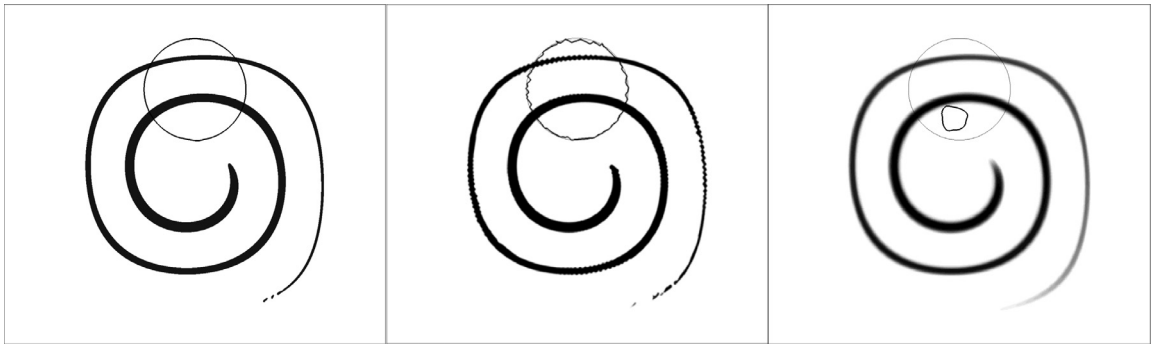

Fig. 6. Results for the 2D vortex on the 512^2 square mesh for (left to right) CLSVOF, standard interFoam solver with compression and without compression. CLSVOF results are shown by LS = 0 isosurface at maximum stretch and at initial and final positions. Results from interFoam are shown by contour of VOF at maximum stretch and VOF = 0.5 isosurface at final position.

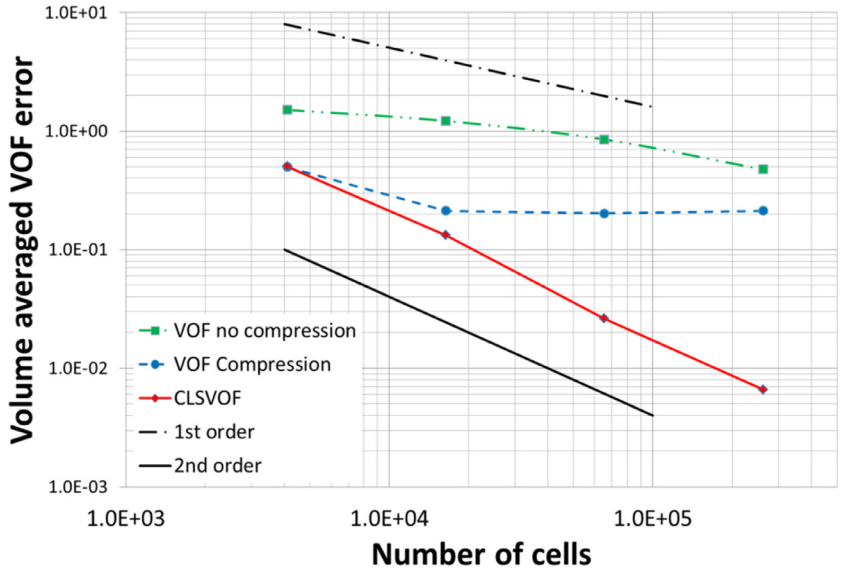

Fig. 7. Volume averaged error of predicted final VOF field for 2D vortex test on successively refined triangular meshes. Results are shown with standard interFoam algebraic VOF solver with and without compression as well as CLSVOF. Also shown are lines to indicate the gradient given by first and second order convergence.

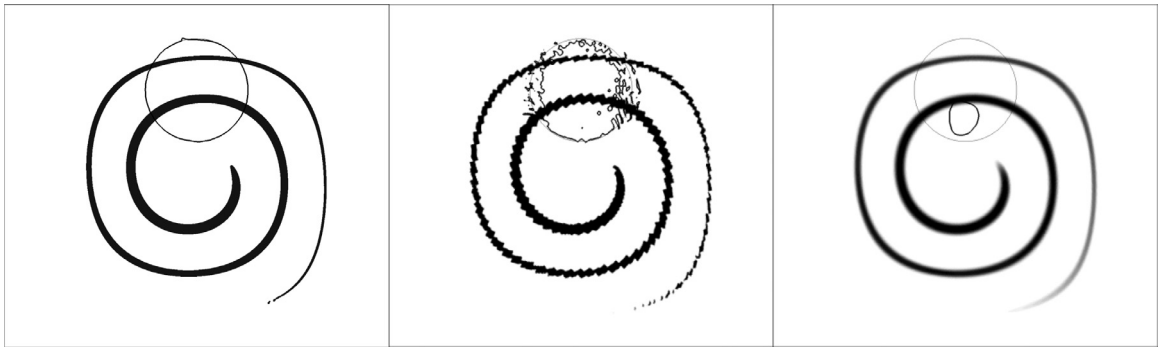

Fig. 8. Results for the 2D vortex on the 512^2 triangle mesh for (left to right) CLSVOF, standard interFoam solver with compression and without compression. CLSVOF results are shown by LS = 0 isosurface at maximum stretch and at initial and final positions. Results from interFoam are shown by contour of VOF at maximum stretch and VOF = 0.5 isosurface at final position.

compared to the Cartesian mesh of the same number of cells the order of convergence for the CLSVOF results is not reduced by a large amount. It can be seen that at high mesh resolutions for this case CLSVOF gives significantly more accurate results than interFoam with compression velocity which show no improvement with increasing resolution. The reason for this can be seen in Fig. 8 which shows the initial and final positions for the three solvers on the finest mesh as well as the maximum stretch using the same format as Fig. 6. The interFoam results with compression can be seen to have a high degree of sharpness at maximum stretch but this has come at the expense of the ligament erroneously breaking up. This then results in a highly distorted shape when it reaches the final position, leading to a large error in the averaged volume field. The CLSVOF solution on the other hand keeps the definition of the ligament which results in improved results at the final step. Computations were also made using CLSVOF both in serial and in parallel. This led to identical results with very accurate mass conservation within machine round off, confirming the correct implementation of the parallelisation.

4.3. Interface capturing test case 2: 3D sphere in uniform flow

As a test of the 3D interface capturing capability a test case of a sphere being transported in a uniform flow was used. A domain of (4,1,1) m is used with a constant uniform velocity of (1,0,0) m/s. A sphere of radius 0.25 is initially placed at (0.5,0.5,0.5) and the simulation is run for a period of T = 3. The final state should be a sphere centred at (3.5,0.5,0.5) m which gives a reference solution for assessing both the error in predicted VOF distribution and interface normal. Simulations were run with the CLSVOF solver as well as interFoam with and without compression velocity. This was carried out firstly with uniform hexahedral meshes of 0.13, 1.0 and 8.0 M cells using time steps of 2×10^{-3}, 1×10^{-3} and 5×10^{-4}s. Results from the three methods on the 1 M cell mesh are shown in Fig. 9. Note that the VOF field for the solver without compression suffers strongly from diffusion which is not shown by the isosurface.

The volume averaged VOF error on the different meshes, as calculated by Eq (24), is shown in Fig. 10. It can be seen that CLSVOF gives an improvement in error for all meshes. The error for the algebraic VOF method without compression can be seen to be significantly higher even though the isosurface in Fig. 9 appears to be a very good representation of the true surface. What cannot be seen in Fig. 9 is the region of cells taking values between 0 and 1 which contribute to the large error seen in Fig. 10. While the absolute level of accuracy has been improved for all meshes with the CLSVOF method it can be seen that both CLSVOF and interFoam results do not show the same order of convergence as in the 2D case in Section 4.2. This is likely to be due to the MULES limiter ensuring boundedness at the expense of accuracy. This is an area that could potentially be improved in further development of our CLSVOF method.

However, one of the main advantages of using a CLSVOF method is that surface normal can be calculated from a continuously differentiable LS field rather than a discontinuous VOF field. To measure the error in normal prediction for the three solvers we find the 'exact' normal vector, $\boldsymbol{n}_{ex}$, using a prescribed LS field centred on the true final position of the sphere (3.5,0.5,0.5) m. The error in the prediction of this can be found from the dot product of this exact normal with the normal predicted from the predicted VOF or LS fields. A mean error for the surface normal can be found as

$$E_n = \frac{1}{N}\sum_{i}^{N} |1 - \boldsymbol{n}_i \cdot \boldsymbol{n}_{ex,i}| \tag{25}$$

Where the average is over all interface cells. For the CLSVOF results we have also compared the error in finding the normal from LS with that from using the VOF field of the same solution. This is shown in Fig. 11. This gives some idea of the improvement in normal prediction using CLSVOF methods compared to geometric VOF methods. Significant improvements can be seen using the LS field over all other methods. The combination of low $E_n$and $E_\propto$ show the ability of the CLSVOF method to combine sharpness and smoothness of the interface.

The same tests were also repeated using unstructured tetrahedral meshes of 0.13, 1 and 8 M cells with time steps of 2×10^{-3}, 1×10^{-3} and 5×10^{-4}s. The final position results for the 1 M cell grids are shown in Fig. 12. Again it should be noted that the VOF field from the interFoam solver without compression suffers from a high degree of numerical diffusion. This can be seen more in the averaged error than the VOF = 0.5 isosurface but it can be seen that the isosurface is distorted. The CLSVOF results reveal some global distortion of the spherical shape but the predicted surface is reasonably smooth when compared to the interFoam results with compression. For the latter it can be seen that while the global shape is conserved well there is a high degree of local distortion.

The errors, calculated as above, are shown in Figs. 13 and 14 and for different mesh sizes. As expected VOF error decreases as the mesh is refined with the solver with no compression showing considerably worse results than the other two methods and CLSVOF showing an improvement over interFoam with compression at all mesh sizes. While the error in VOF field with the interFoam solver compares fairly well with CLSVOF the comparison of error in prediction of normal vector shows the effect of the local distortion of the surface seen in Fig. 12. It can be seen that the error for this solver increases with mesh size as these distortions are

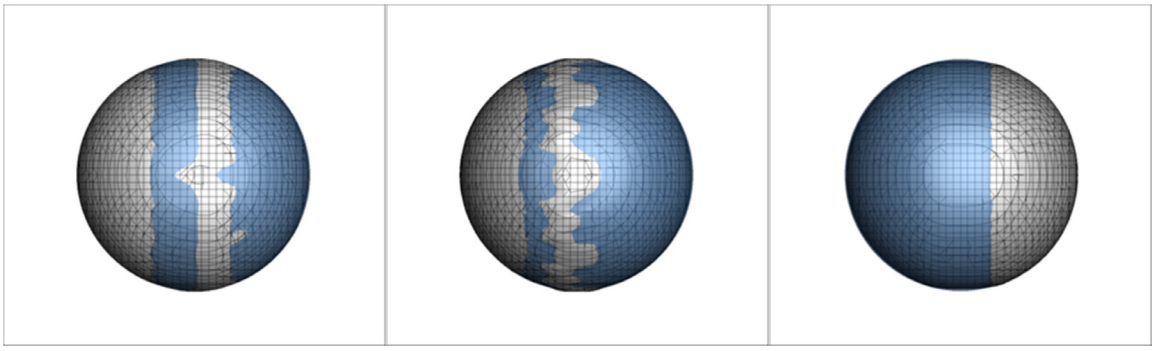

Fig. 9. Sphere in uniform flow after $t = 3$ s on 1 M cell hexahedral mesh. Left to right, CLSVOF LS = 0 isosurface, interFoam with compression VOF = 0.5 isosurface and interFoam without compression VOF = 0.5 isosurface. Blue sphere is exact solution.

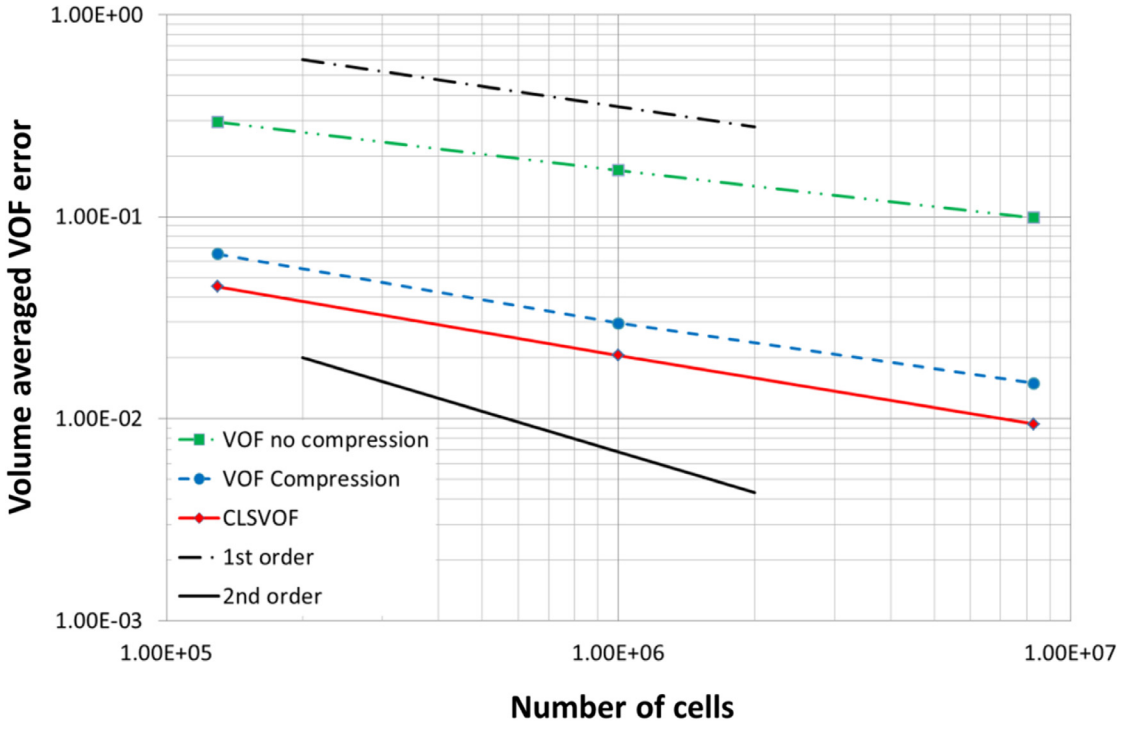

Fig. 10. Volume averaged error of predicted final VOF field for 3D sphere test on successively refined hexahedral meshes. Results are shown with standard interFoam algebraic VOF solver with and without compression as well as CLSVOF. Also shown are lines to indicate the gradient given by first and second order convergence.

amplified by the decreased cell size. The surface normal error for the interFoam results without compression appears to be good, but this is the effect of diffusion of the interface leading to a smoothed VOF field. The VOF and surface normal errors with all solvers are inferior to those found on a hex mesh which shows the importance of using high quality meshes where possible. However the CLSVOF solver is seen to be a significant improvement over the standard interFoam solver for prediction of surface normal, and hence curvature, suggesting that it may be advantageous for cases where tetrahedral meshes are deemed necessary. The accurate prediction of surface normal can be expected to be important when coupled with the momentum solver for real two phase flow problems as this will feed directly into the calculation of the surface tension.

4.4. Interface capturing test case 3: 3D deformation of a sphere

A 3D test case proposed in LeVeque (1996) and also applied by Ménard et al. (2007) was used to evaluate the 3D CLSVOF interface capturing algorithm. A sphere of radius 0.15 is placed within the domain $[0, 1]^3$ with its centre at (0.35, 0.35, 0.35). The velocity field is specified by

$$u(x, y, z, t) = 2\sin^2(\pi x)\sin(2\pi y)\sin(2\pi z)\cos(\pi t/T) \quad (26)$$

$$v(x, y, z, t) = -\sin^2(\pi y)\sin(2\pi x)\sin(2\pi z)\cos(\pi t/T) \quad (27)$$

$$v(x, y, z, t) = -\sin^2(\pi z)\sin(2\pi x)\sin(2\pi y)\cos(\pi t/T) \quad (28)$$

where $T = 3$ s is the period. With this test case, the liquid sphere stretches into a thin film. In the full test the sphere deforms up to $t = 1.5$ s before returning to its original shape at $t = 3$ s. As the full calculation on a sufficiently refined tetrahedral mesh can be expensive we have instead taken the shape at $t = 1$ s as being sufficiently deformed to be used as a verification for the CLSVOF interface capturing implementation. This has been done on only one mesh with the intention being to demonstrate that the method is capable of working on a tetrahedral mesh for a significantly deformed shape. A 3D unstructured tetrahedral mesh of around 3.5 M elements was used with computations carried out on 64 processors. Fig. 15 compares the results of the predictions with the exact

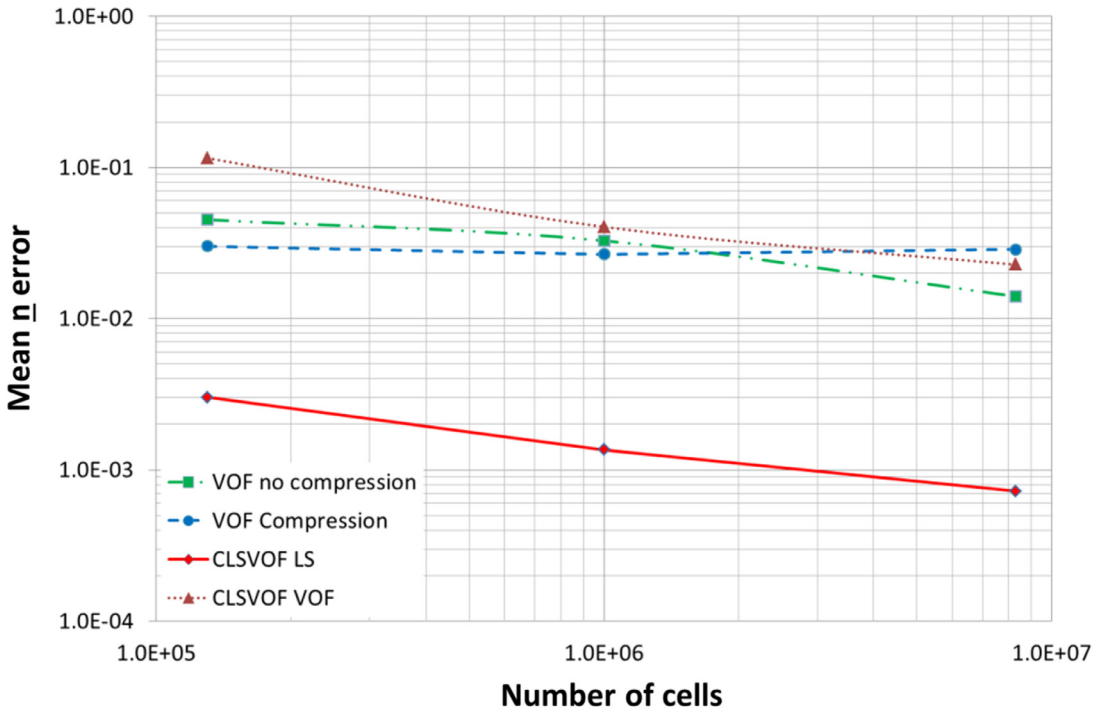

Fig. 11. Average surface normal error VOF field for 3D sphere test on successively refined hexahedral meshes. Results are shown with standard interFoam algebraic VOF solver with and without compression as well as CLSVOF. Also shown are results using the gradient of the VOF field in the CLSVOF solution.

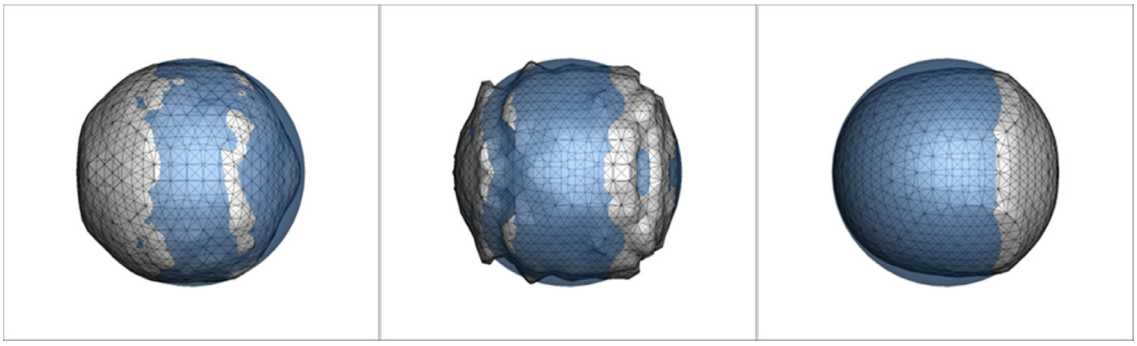

Fig. 12. Sphere in uniform flow after $t=3$ on 1 M cell tetrahedral mesh. Left to right, CLSVOF LS = 0 isosurface, interFoam with compression VOF = 0.5 isosurface and interFoam without compression VOF = 0.5 isosurface. Blue sphere is exact solution.

solution characterised by the dots on the liquid surface. A solution for comparison was found by locating 20,000 particles at random locations on the surface of the initial sphere. Their position, and hence that of the surface, over time was then found by integrating Eqs (26-28) for their position using a separate ODE solver with a time step of 0.1 ms. The particles' positions at $t=1$ s can then be overlaid with the CLSVOF isosurface to compare the prediction from the two methods. The excellent agreement seen in Fig. 15 confirms the accuracy of the current interface capturing algorithm when used for a 3D tetrahedral mesh.

5. Test case: impacting drop

In order to validate the full implementation of the CLSVOF model with the momentum solver and contact angle models, the experimental data of Yokoi et al. (2009) for the behaviour of a droplet impacting on a dry surface was used. This was also used as the test case by Griebel and Klitz (2013) using the same contact angle models. In this experiment a spherical water drop of 2.28 mm diameter impacts a solid surface with an impact speed of 1 m/s. The substrate is a silicon wafer onto which hydrophobic silane is grafted using standard microelectronic procedures. The surface roughness is less than 50 nm. The surface tension is 0.072 N/m, the air and liquid densities are 1.25 kg/m^3 and 1000 kg/m^3 respectively and the dynamic viscosities of air and liquid are 1.82e−5 Pa.s and 0.001 Pa.s. The flow in both phases is assumed to be laminar. Detailed measurements are available for the equilibrium ($\theta_s = 90°$) as well as static and dynamic advancing and receding contact angles.

5.1. Comparison of interFoam and CLSVOF results for orthogonal mesh

Solutions were first obtained using a three dimensional Cartesian orthogonal mesh. The solution domain is 7.4 x 3.7 x 7.4 mm in the x, y and z directions respectively. The mesh used for both interFoam and CLSVOF is a hexahedral mesh of 100 x 80 x 100 in the corresponding directions being uniform on the horizontal planes but refined near the wall in the vertical direction with the expansion ratio of around 1.02. The ability to use stretched meshes of this sort is a useful feature of the arbitrary grid formulation used here. The mesh resolution near the wall is such that there are re-

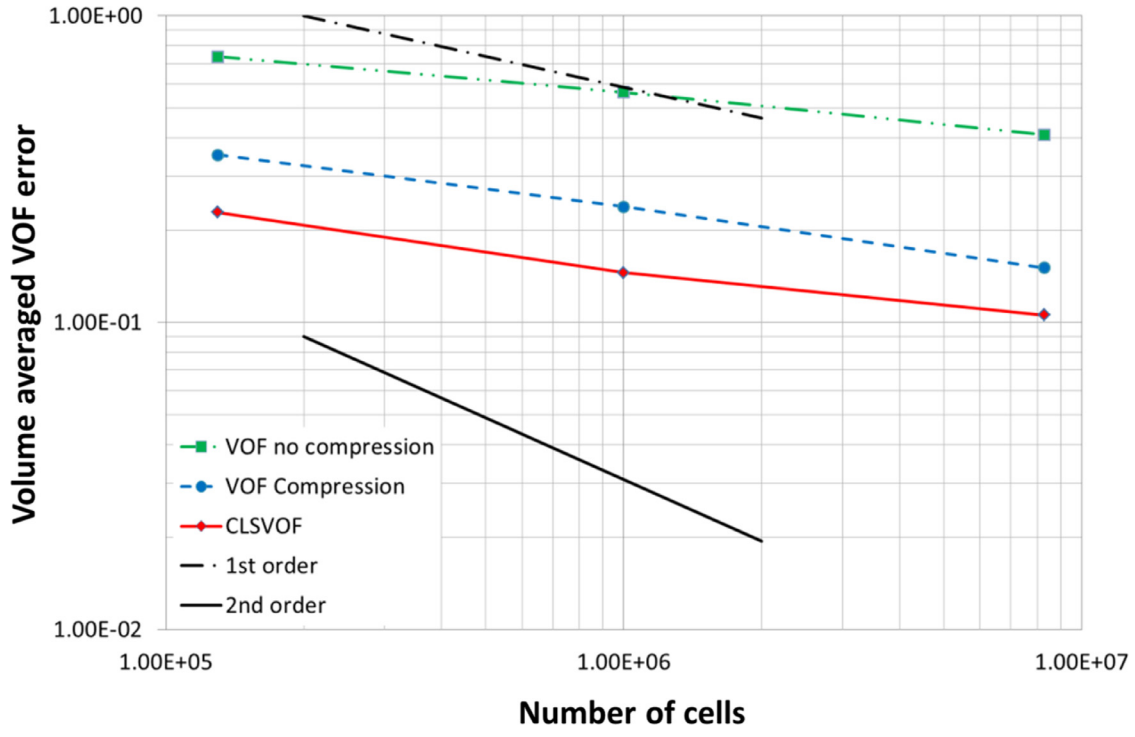

Fig. 13. Volume averaged error of predicted final VOF field for 3D sphere test on successively refined tetrahedral meshes. Results are shown with standard interFoam algebraic VOF solver with and without compression as well as CLSVOF. Also shown are lines to indicate the gradient given by first and second order convergence.

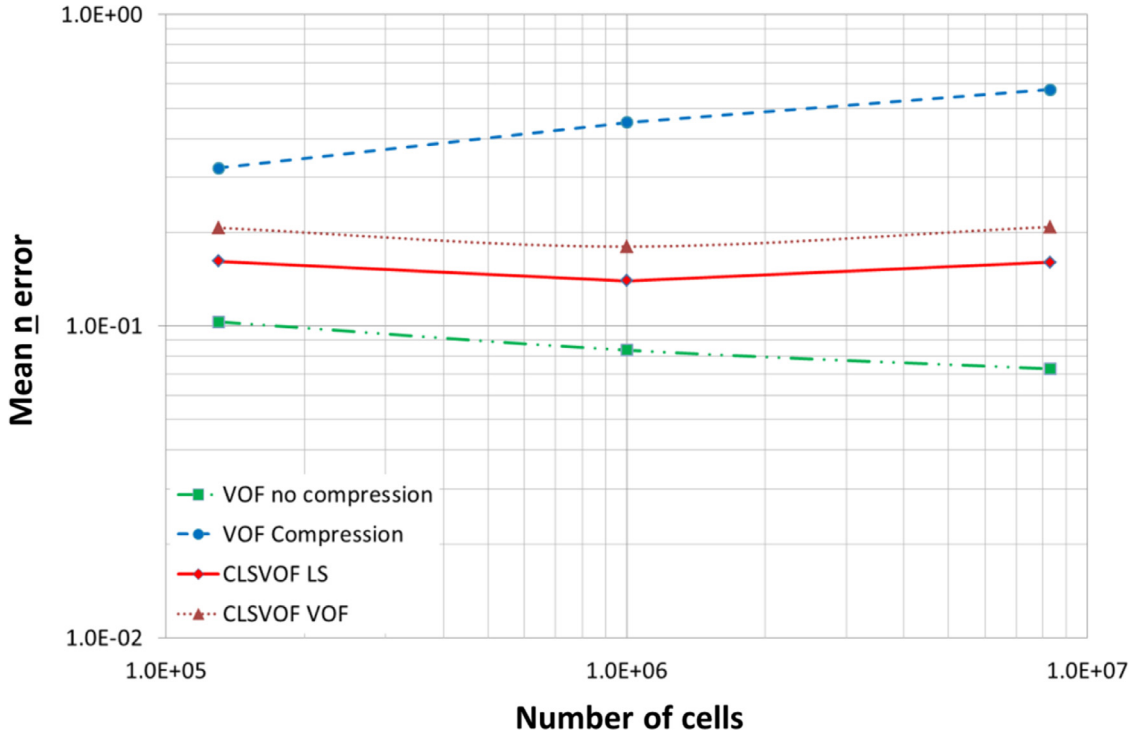

Fig. 14. Average surface normal error VOF field for 3D sphere test on successively refined tetrahedral meshes. Results are shown with standard interFoam algebraic VOF solver with and without compression as well as CLSVOF. Also shown are results using the gradient of the VOF field in the CLSVOF solution.

spectively 5 and 17 cells across the thinnest and the thickest part of the film when drop attains its maximum diameter at $t \sim 4$ ms. In situations where the near wall resolution used in the numerical analysis differs from the macroscopic length associated with the specified contact angle, corrections need to be applied to the contact angles that are imposed as the boundary conditions. Afkhami et al. (2009), for example, have developed a grid dependent correction procedure based on Cox (1986) analysis that leads to grid independent solutions. Their model allows smaller numerical resolution compared to macroscopic scale associated with the apparent contact angle while still significantly large in comparison with microscopic scale. However, such a slip model has not been incor-

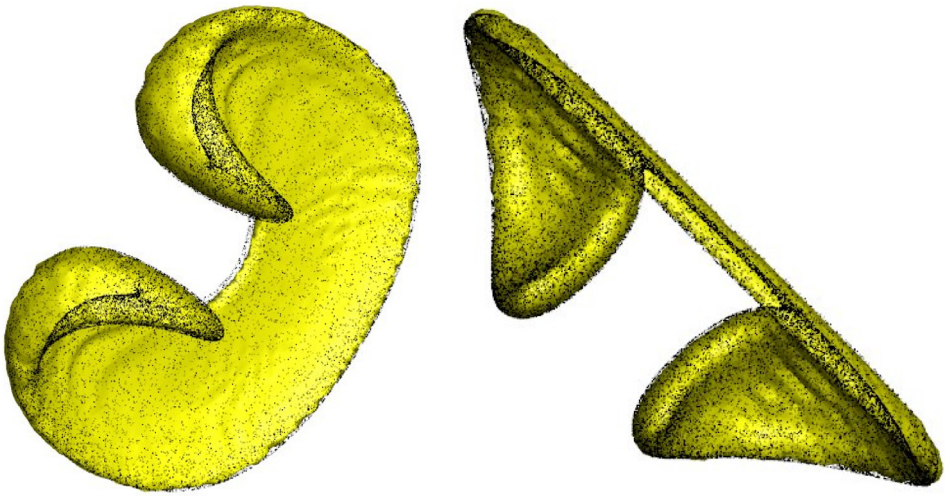

Fig. 15. Deformation of a sphere in a 3D vortex field after $t = 1$ s. Isosurface of LS = 0. Dots represent exact Lagrangian solution.

porated in the current numerical simulation and hence care must be taken to use suitable wall proximity grid spacing. The value chosen is $\Delta = 0.02$ mm based on the experimental observations that give a recommendation for the choice of macroscopic length $\Delta/2 \sim 10^{-5} - 10^{-4}$ m (Legendre and Maglio 2013; Maglio and Legendre 2014). This is also consistent with the fine 200×200 grid used in Yokoi et al 2D numerical analysis. They report little grid sensitivity within 50×50 and 200×200 mesh size range in their numerical simulation. In order to investigate the grid dependence here, the solution is also obtained for CLSVOF on a coarser $50 \times 50 \times 50$ grid. For this mesh the domain is $10 \times 5 \times 10$ mm and the size of the cell in proximity to the wall is a little more than twice the size for the finer mesh ($\Delta \sim 0.045$ mm) but still within acceptable macroscopic length scale. This leads to 3 and 9 cells across the thinnest and the thickest section of the film at the maximum contact patch time.

A constant pressure is imposed on the top plane which allows inflow and outflow. At this boundary a zero gradient is assumed for VOF and LS. Elsewhere wall boundary conditions are applied with no-slip condition for velocity and zero gradient for pressure. The dynamic contact angle model from Yokoi et al, described by Eq. (20) in Section 3, was implemented in OpenFOAM and applied in the simulation. For the coarse mesh a fixed timestep of $\Delta t = 1.0 \times 10^{-6}$s was used. For the fine mesh both interFoam and CLSVOF calculations used a fixed time step of $\Delta t = 2.5 \times 10^{-7}$s. Calculations were made on 16 Intel Sandy Bridge 2.0 GHz CPUs and the total execution time for the interFoam (VOF) calculation was 68 h while that for the CLSVOF solver was 72 h. It is likely that this increase in time is small due to this problem having a relatively small number of interface cells meaning that the most significant cost is the pressure correction solver which is common to both methods. Cases with a greater degree of stretching may see a bigger penalty due to the bisection algorithm used for reconstruction and improved iterative methods may be necessary. The results confirmed very accurate mass conservation, found by volume integration of the VOF field, of better than ±0.05% for all models investigated. This confirms the mass conservative nature of the CLSVOF implementation used here which would be necessary for practical automotive EWM applications as discussed in Section 1.

In Fig. 16 the experimental time variations in drop shape is compared with the interFoam and the CLSVOF predictions using the Yokoi et al contact angle model, as this is derived using data from this experiment. The surfaces shown are LS = 0 for CLSVOF and $\alpha = 0.5$ for interFoam. Note that a different choice of α can be made which would change the appearance. A very close agreement between the coarse and fine CLSVOF solutions confirms that grid used is sufficiently fine. The results presented hereafter are based on the fine mesh solution unless otherwise stated. Predictions with both models are in reasonable qualitative agreement with the data although CLSVOF results are in closer accord, in particular at 10 ms. As shown in Fig. 17, interFoam predicts an air bubble trapped within the drop. Such a feature is not consistent with the experimental observation. The air bubble in the interFoam result is caused by a dry patch created during the rebounding process due to a lack of resolution of the interface position close to the surface. With the CLSVOF prediction there is no indication of any air bubble trapped within the drop, which shows the importance of accurate interface capturing. These results also validate the numerical implementation of the CLSVOF method with the momentum solver and contact angle model boundary condition.

In order to provide a quantitative comparison of the results, the variation of contact patch diameter with time is presented in Fig. 18. Experimental data and results with interFoam and CLSVOF solvers are shown together with the theoretical equilibrium diameter. Note a very close agreement between the coarse and fine mesh results for the CLSVOF confirming once again very little dependence on the grid resolution used. It is clear that with the Yokoi et al contact angle model both interFoam and CLSVOF give reasonable results with both predicting the correct steady state diameter. However it can be seen that the CLSVOF results are superior, giving a very accurate prediction of the initial spreading and receding of the droplet including the peak diameter which the interFoam solver over predicts. CLSVOF also shows a superior prediction of the period approximately 12–18 ms where the contact patch diameter remains constant. The relative inaccuracy of the interFoam method is likely to be due to two factors. Firstly the ambiguity in the exact location of the contact patch created by the need to choose an arbitrary VOF value to define the surface. Secondly the greater interface resolution offered by the CLSVOF allows the contact angle to be resolved more accurately which in turn will affect the forces exerted on the droplet. The quality of the results using the 50x50x50 grid highlights the advantages of the CLSVOF method. Accurate results are obtained here with CLSVOF, whereas for the interFoam solver the results are noticeable inferior on the coarse mesh with neither the peak diameter nor the equilibrium diameter predicted well due to the poor interface capturing. This is likely to be a significant benefit if the method is applied to more

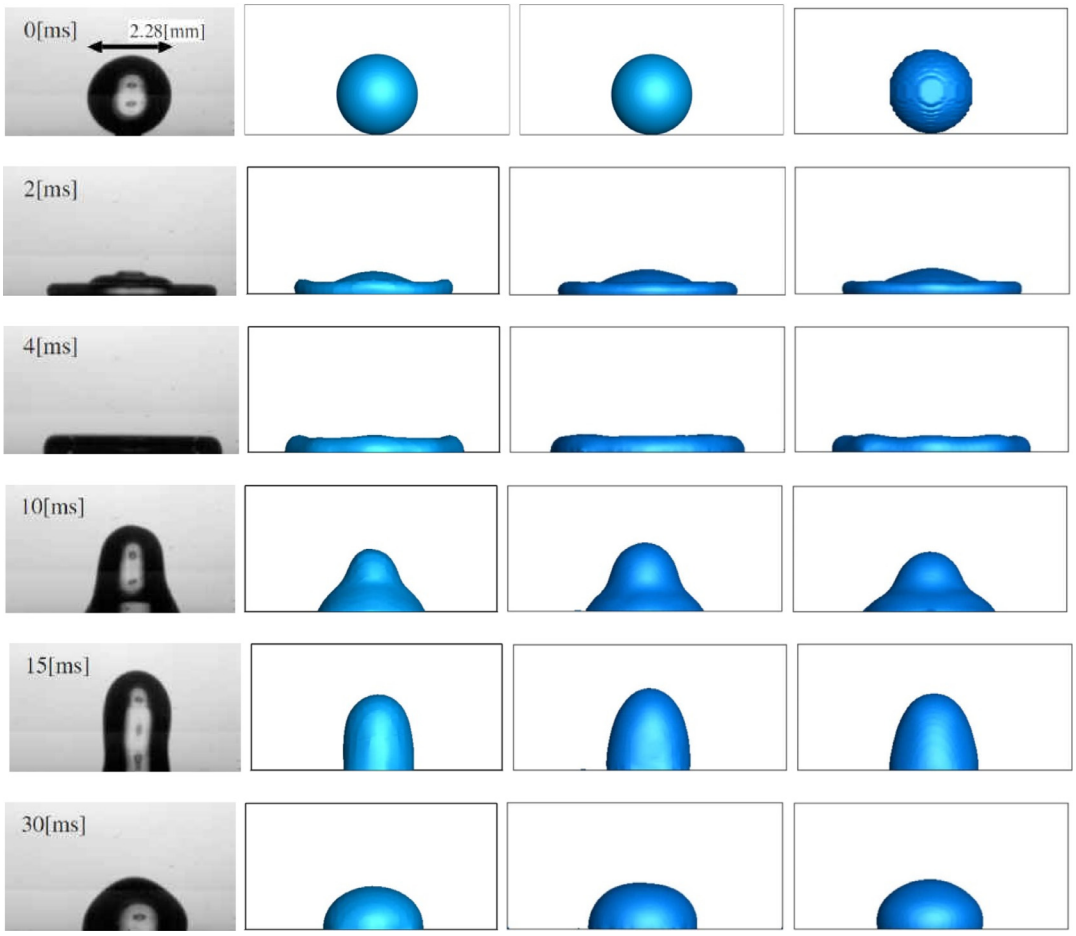

Fig. 16. Drop shape variation vs. time. From left to right: Exp (Yokoi et al. 2009), CLSVOF coarse mesh, CLSVOF fine mesh, interFoam fine mesh ($\alpha = 0.5$ isosurface). All simulations use Yokoi contact angle model.

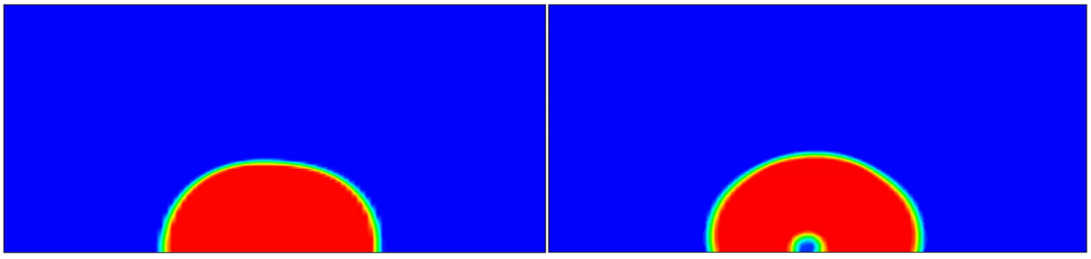

Fig. 17. Contours of VOF through centre of drop with Yokoi contact angle mode at t = 30 ms: CLSVOF solver (left) vs. interFoam solver (right).

complex problems such as those encountered with vehicle surface flows.

5.2. CLSVOF results simulation using 'O-Ring' mesh

As discussed in Section 1 our ultimate motivation for implementing the CLSVOF method in an unstructured, multi-purpose code such as OpenFOAM is to allow it to be used for surface liquid flows with more complex geometry. Highly skewed or distorted meshes will always lead to less accurate results and so attention must still be paid to mesh quality even in unstructured meshes. Therefore having validated CLSVOF performance using an orthogonal Cartesian mesh we now attempt to validate its performance on a block-structured curvilinear 'o-ring' type mesh. This type of mesh is particularly well suited to the 3D representation of an axisymmetric case such as this. The mesh used is shown in Fig. 19 and consists of a central block of 70 x 70 elements surrounded by four blocks with 42 elements in the radial direction. A total of 80 rows in the vertical direction are used leading to approximately 1.3 M elements. The variable time step option was used with global and interface Courant numbers set to 0.2. Similar to the Cartesian orthogonal fine mesh, the near wall mesh spacing is $\Delta = 0.02$ mm with the expansion ratio of 1.05. Note that the mesh elements, while still hexahedral, are no longer cuboid in shape particularly at the edges of the blocks. Therefore the clipping and capping algorithm is required to reconstruct the interface location. The boundary conditions and other setup parameters were set to be the same as in the Cartesian case in Section 5.1.

Fig. 20 shows the variation with time of the droplet shape predicted by CLSVOF on this mesh. Comparison with Fig. 16 shows that the predictions with the o-ring mesh are very similar to those produced using the orthogonal mesh. These results show that the

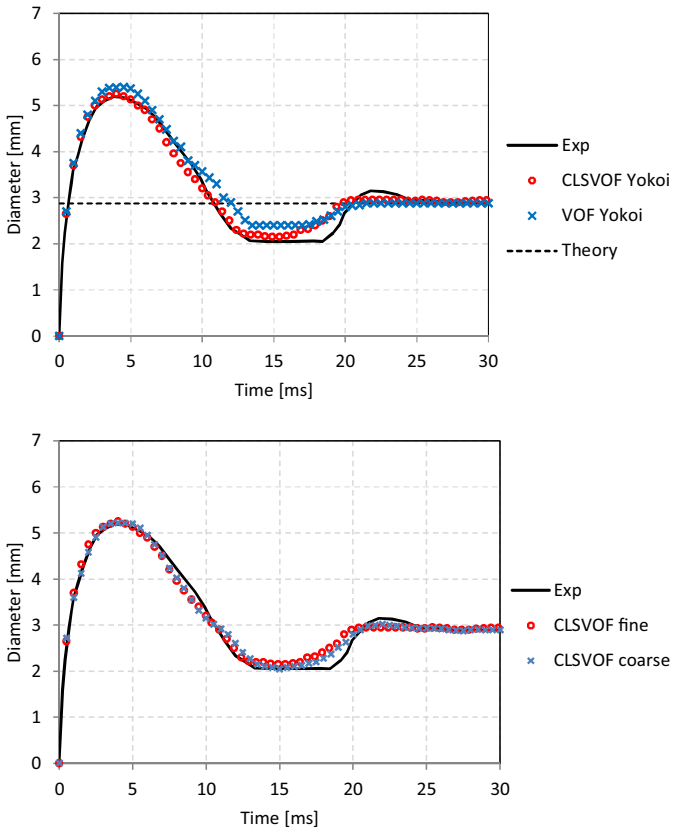

Fig. 18. Time variation of droplet contact patch diameter with Yokoi contact angle model. Top: interFoam algebraic VOF solver vs. CLSVOF, bottom: CLSVOF with coarse and fine mesh. Experimental data from Yokoi et al. (2009).

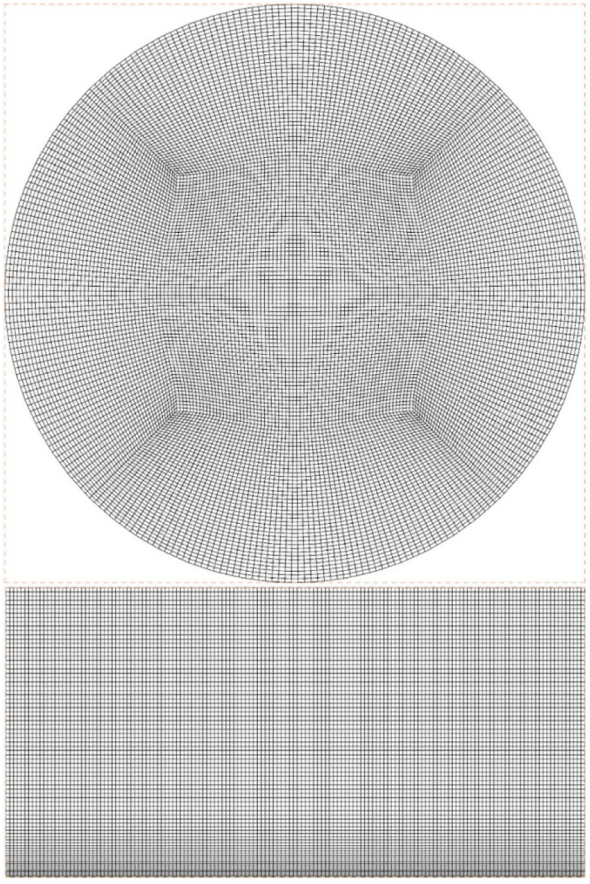

Fig. 19. 'O-Ring' type mesh used for simulation of impacting droplet, view from above (top) and from the side (bottom). Domain diameter is 10 mm and height 5 mm.

full CLSVOF method implemented in OpenFOAM, with momentum coupling and high fluid density ratios, is capable of successfully producing results on non-Cartesian meshes. The accuracy of the method using this grid is further confirmed by Fig. 21 which shows the temporal evolution of contact patch diameter from the o-ring mesh prediction compared with experimental data. Again we see a close level of agreement with experiment, confirming that if a suitable contact angle model is supplied that the CLSVOF method implemented here is capable of producing accurate results with non-Cartesian meshes.

6. Droplet flow over channel with curved edges

Now that the accuracy of the method has been demonstrated, subject to an accurate contact angle model, in this section we present results to demonstrate the ability of the CLSVOF method to simulate free surface flow over curved geometry. Simulations have been performed of a water droplet of volume around 53 mm^3 approaching a square channel of width 3 mm with curved edges on a 30° slope. This is representative of an exterior water management feature as might found on a road vehicle. It is an example of a simulation for which typical fluid film models would not

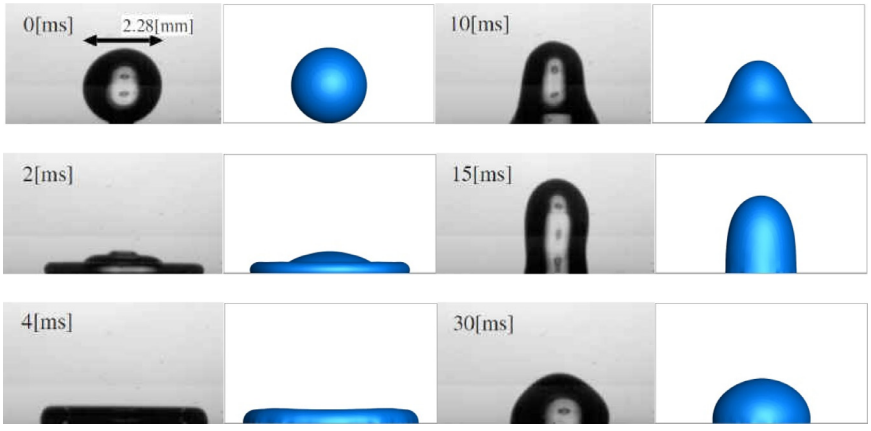

Fig. 20. Drop shape variation vs. time. Left: experimental (Yokoi et al. 2009), right: CLSVOF LS = 0 using 'O-Ring' mesh with Yokoi contact angle model.

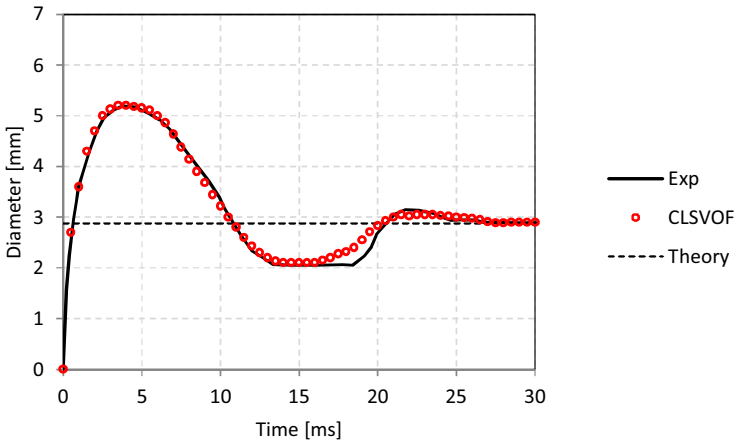

Fig. 21. Time variation of droplet contact patch diameter using CLSVOF on 'O-Ring' mesh with Yokoi contact angle model. Experimental data from Yokoi et al. (2009).

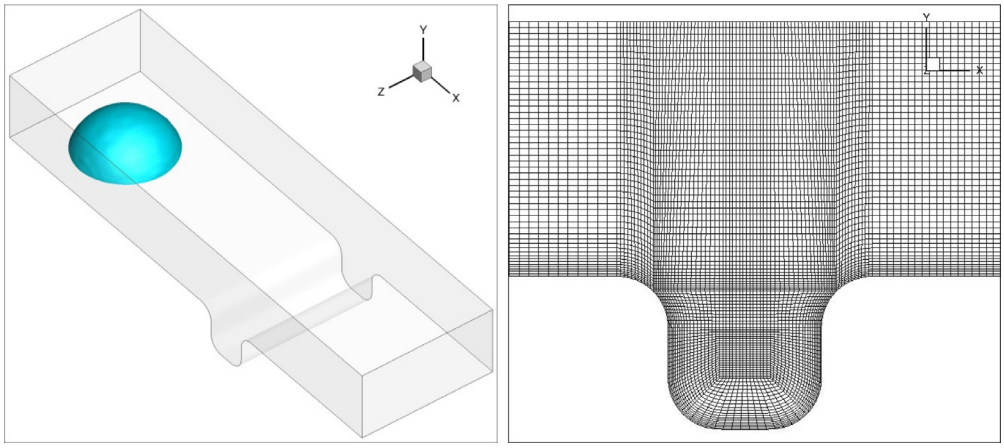

Fig. 22. Starting shape and position of droplet on plate for hydrophilic surface (left) and mesh used for the curved channel geometry (right).

be appropriate; the droplet has dimensions similar to that of the channel and velocities normal to wall will be significant making the assumptions of the thin film model invalid. To predict whether the droplet leaves the surface at the edge of the channel with film models would also require empirical models with prior calibration.

The Cox–Voinov contact angle model of Eq. (14) has been used with static contact angles of $\theta_s = 135^\circ$ and $\theta_s = 70^\circ$ to represent generic hydrophobic and hydrophilic surfaces respectively. For each case, drop shape is initialised using spherical cap that matches drop volume and its static contact angle. To bound the simulation the channel is of finite width with the side walls of the domain set to have the same contact properties as the slope. The initial velocity of the droplet is zero and it subsequently moves under gravity. The mesh used is shown in Fig. 22 together with the starting shape and position of the droplet for $\theta_s = 70^\circ$ test case. The near wall cell thickness is 0.03 mm which is similar to that used for the previous impinging drop test. The total number of cells is 0.56 M This is an example of a geometry that could not be simulated using a CLSVOF formulation suitable only for orthogonal meshes. An 'o-ring' mesh has again been employed which allows the curved edges of the channel to be captured. Fig. 22 shows that this mesh has led to several areas of significantly non-orthogonal cells where the iterative clipping and capping algorithm used here for interface reconstruction is required.

Fig. 23 shows the motion of the drop on two surfaces characterised by two contact angles. The contact angles are used here to represent the motion of water drops over generic hydrophobic and hydrophilic surfaces. This is done to demonstrate the ability of CLSVOF to show the differences in droplet behaviour due to a change in the surface properties. While the two contact angles used do not represent specific surfaces we have seen in Section 5 that correct droplet dynamics can be predicted if accurate macroscopic contact angle data is available. For comparison the case was also repeated using the standard interFoam solver with the compression velocity active. These results are shown in Fig. 24 where the interface is visualised using VOF = 0.5.

The channel filling process with the hydrophilic surface is predicted to be slightly different with the interFoam results, which is visible at 100 ms. However the biggest difference is seen for the hydrophobic surface where the interFoam solver predicts the droplet to break into two, unlike with the CLSVOF solver where it remains intact. This difference can be explained by viewing the predicted VOF contours through the centre of the drop at 103 ms in Fig. 25. Here it can be seen that, while in the CLSVOF results the interface is kept sharp, the interface in the interFoam simulation has become smeared over several cells. This inaccuracy in interface definition will also lead to an inaccuracy in the surface tension term. The result of this is that the tail of the droplet becomes detached in the VOF simulation. Given the increased accuracy for both surface location and normal seen in the verification and validation tests we can be confident that the CLSVOF result is showing the more correct result.

The CLSVOF implementation employed here is seen to be capable of simulating free surface flows on curved geometry and showing the effect of changing surface properties. The droplet on the hydrophilic surface is seen to approach the channel more slowly

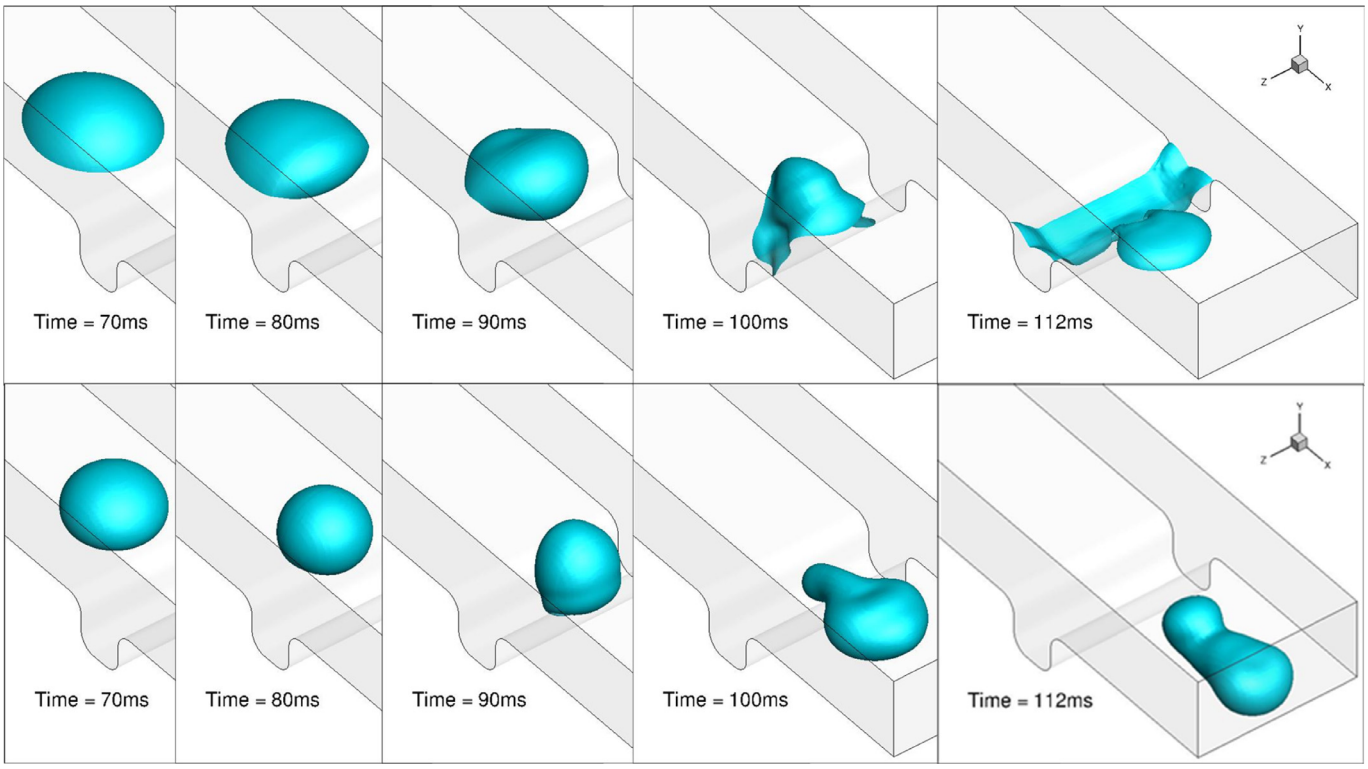

Fig. 23. Instantaneous images from CLSVOF simulations of water droplet flowing across a channel with rounded corners: top, hydrophilic surface; bottom, hydrophobic surface.

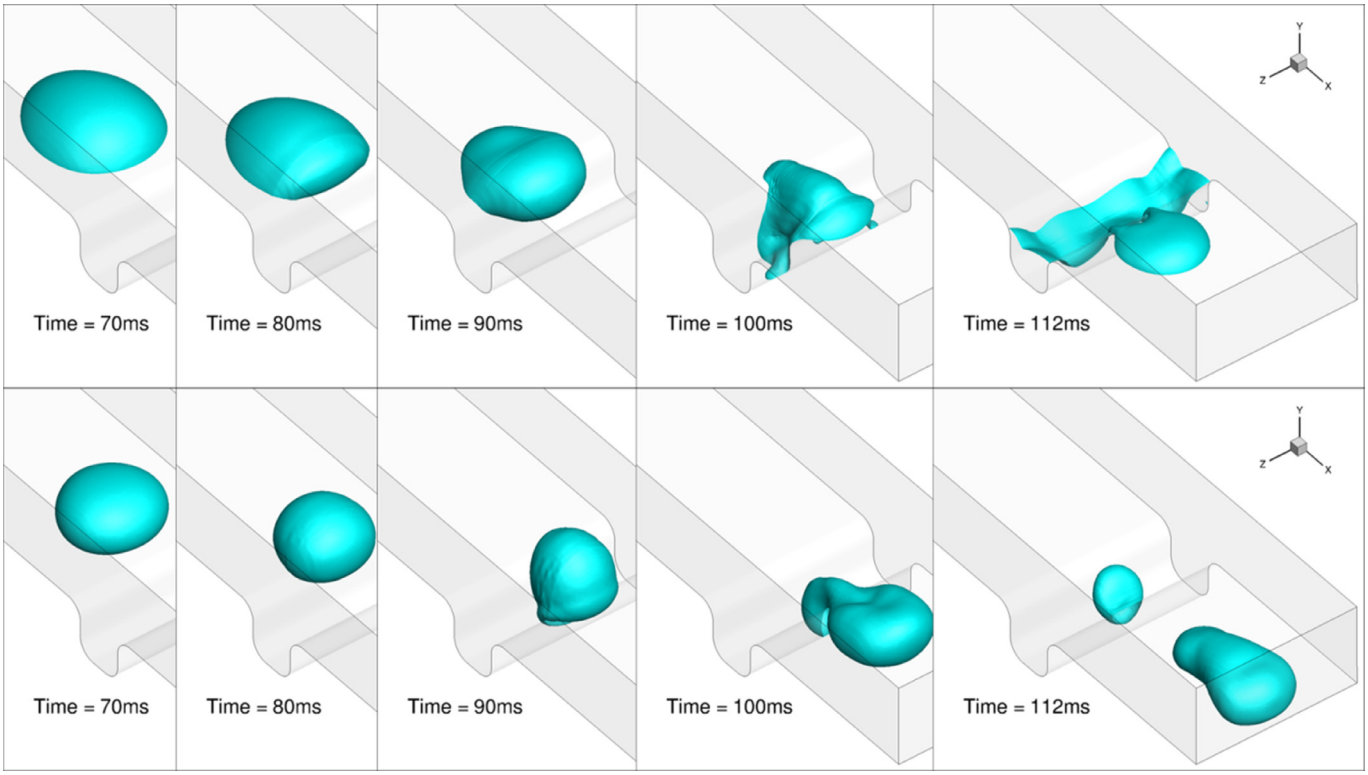

Fig. 24. Instantaneous images from interFoam simulations of water droplet flowing across a channel with rounded corners: top, hydrophilic surface; bottom, hydrophobic surface.

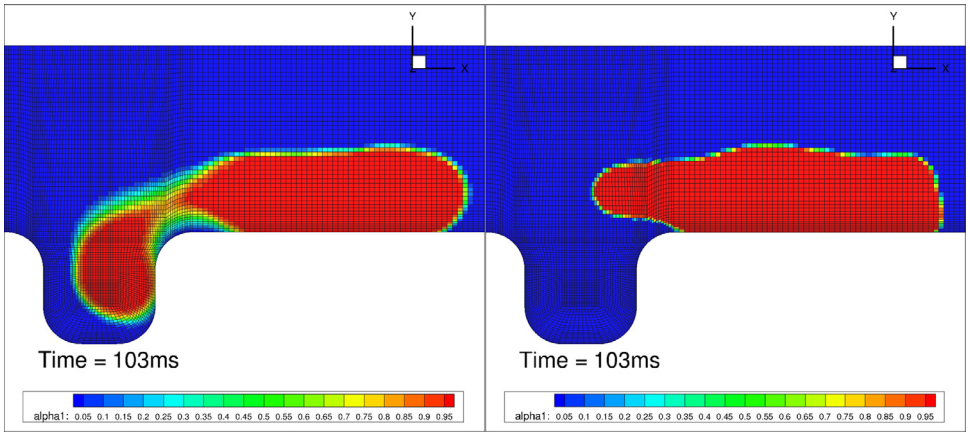

Fig. 25. Contour of VOF field from interFoam with compression (left) and CLSVOF results (right) through centre of drop flowing over hydrophobic surface.

and then to fill the channel with a small overspill. On the hydrophobic surface the droplet approaches more quickly and is able to clear the channel as an intact droplet. Being able to predict such changes would be valuable when designing surface water management feature. The use of CLSVOF allows for mass conservation while still maintaining a sharp interface definition in order to do this.

7. Conclusions

The motivation for this work is the desire for a predictive tool to investigate exterior water management on road vehicles. This tool is required to have the ability to accurately resolve the surface of flows such as droplets and rivulets while conserving mass. It should also be capable of including the effect of water travelling over different surfaces through appropriate models for dynamic contact angles. It is also desirable for this to be used with unstructured meshes for complex geometry and parallel operation so that it can be used for realistic cases. To this end of the CLSVOF method for use with arbitrary unstructured grids has been implemented into the OpenFOAM CFD suite together with a contact angle model. The implementation has been verified using a series of test cases. The re-initialisation routine for unstructured grids has been shown to return an initially distorted level-set field to a signed distance function in the interface vicinity without changing the interface location. The model has been seen to provide excellent mass conservation for all cases tested in both serial and parallel operation. For a 2D vortex test the CLSVOF solver was seen to give superior results to the standard algebraic VOF solver interFoam on both square and triangular meshes. For the triangular mesh it was seen that the use of an algebraic VOF solver with a compression term led to a highly distorted interface, unlike the CLSVOF solver which maintained the shape well. For a convected sphere case the CLSVOF solver was seen to give improved results for both surface position and particularly normal vectors compared to interFoam on both hexahedral and tetrahedral meshes. Again CLSVOF was seen to retain a smoother sphere than interFoam with compression term which again predicted a locally distorted surface with the tetrahedral mesh.

To validate the full implementation with the momentum solver the method is compared, using the same mesh for each, to interFoam for the experimental case of a droplet impinging onto a solid surface, which can be taken as representative of the sort of application which may be encountered in automotive applications. A suitable contact angle due to Yokoi et al. (2009) has been implemented for both VOF and LS fields. The CLSVOF method is able to show better agreement than interFoam with experiment for the variation of contact patch diameter. This is due to the unambiguous interface location provided by the zero level-set iso-surface and the better resolution of the contact angle at the surface. The interFoam method is also seen to develop a trapped air bubble in the drop which is not seen in experiment or in the CLSVOF results. The CLSVOF method is furthermore shown to give accurate results on both Cartesian and a non-Cartesian 'O-Ring' type mesh. When the Yokoi model, which is derived by fitting a curve to data for Capillary number and macroscopic contact angle from the same experiment, is used excellent agreement is observed with experiment. This is encouraging as it suggests correct dynamic behaviour of water on a vehicles surface can be predicted if suitable data for macroscopic contact angle is available. It is, therefore, important that such data be obtained experimentally for relevant vehicle surfaces. The validated method has then been applied to water droplets flowing over a drainage channel with rounded edges. This is an example of a case that requires a 3D interface resolving method using a non-orthogonal mesh formulation and is a demonstration of the type of real world application that this method can be used for in future work.

Acknowledgements

This work was supported by Jaguar Land Rover and the UK-EPSRC grant EP/K014102/1 as part of the jointly funded Programme for Simulation Innovation. The authors would like to gratefully acknowledge the guidance given by Mr Adrian Gaylard of Jaguar Land Rover on the subject of vehicle exterior water management and Prof Jim McGuirk of Loughborough University for his advice and comments on the manuscript.

References

Ahn, H.T., Shashkov, M., 2008. Geometric algoriths for 3D interface reconstruction. In: Proceedings of the 16th International Meshing Roundtable. Springer Berlin Heidelberg, pp. 405–422.
Afkhami, S., Zaleski, S., Bussmann, M., 2009. A mesh-dependent model for applying dynamic contact angles to VOF simulation. J. Comp. Phys. 228, 5370–5389.
Albadawi, A., Donoghue, D.B., Robinson, A.J., Murray, D.B., Delauré, Y.M.C., 2013. Influence of surface tension implementation in volume of fluid and coupled volume of fluid with level set methods for bubble growth and detachment. Int. J. Multiphase Flow 53, 11–28.
Arienti, M., Sussman, M., 2014. An embedded level set method for sharp-interface multiphase simulations of Diesel injectors. Int. J. Multiphase Flow 59, 1–14.
Brackbill, J.U., Kothe, D.B., Zemach, C., 1992. Continuum method for modelling surface tension. J. Comp. Phys. 100, 335–354.
Cox, R.G., 1986. The dynamics of spreading of liquids on a solid surface. Part 1. Viscous flow. J. Fluid Mech. 168, 169–194.
Cox, R., 1998. Inertial and viscous effects on dynamic contact angles. J. Fluid Mech. 57, 249–278.
Deshpande, S.S., Anumolu, L., Trujillo, M.F., 2012. Evaluating the performance of the two-phase flow solver interFoam. Comput. Sci. Discovery 5, 014016.

Diot, S., François, M.M., 2016. An interface reconstruction method based on an analytical formula for 3D arbitrary convex cells. J. Comp. Phys. 305, 63–74.
Dupont, J.B., Legendre, D., 2010. Numerical simulation of static and sliding drop with contact angle hysteresis. J. Comp. Phys. 229, 2453–2478.
Dussan, V., E., B., 1979. On the spreading of liquids on solid surfaces: static and dynamic contact lines. Annu. Rev. Fluid Mech. 11, 371–400.
Gaylard, A., Fagg, M., Bannister, M., Duncan, B., 2012. Modelling a-pillar water overflow: developing CFD and experimental methods. SAE Technical Paper 2012-01-0588. SAE Int. J. Passenger Cars – Mech. Syst. 5 (2).
Griebel, M., Klitz, M., 2013. Simulation of droplet impact with dynamic contact angle boundary conditions. In: Singular Phenomena and Scaling in Mathematical Models. Springer, Switzerland, pp. 297–325.
Hagemeier, T., Hartmann, M., Thévenin, D., 2011. Practice of vehicle soiling investigations: a review. Int. J. Multiphase Flow 37, 860–875.
Hoffman R., L., 1975. A study of the advancing interface. I. Interface shape in liquid–gas systems. J. Colloid Interface Sci. 50, 228.
Jilesen, J., Spruss, I., Kuthada, T., Wiedemann, J. and Gaylard, A. 2015. Advances in modelling a-pillar overflow. SAE Technical Paper 2015-01-1549.
Legendre, D., Maglio, M., 2013. Numerical simulation of spreading drops. Colloids Surfaces 432, 29–37 ISSN 0927-7757.
LeVeque, R.J., 1996. High-resolution conservative algorithms for advection in incompressible flow. SIAM J. Numer. Anal. 33 (2), 627–665.
López, J., Hernández, J., 2008. Analytical and geometrical tools for 3D volume of fluid methods in general grids. J. Comp. Phys. 227, 5939–5948.
Maglio, M., Legendre, D., 2014. Numerical simulation of sliding drops on an inclined solid surface. In: Computational and Experimental Fluid Mechanics with Applications to Physics, Engineering and Environment. Springer, p. 47.
Marić, T., Marschall, H. and Bothe, D. 2013. vofFoam – a geometrical volume of fluid algorithm on arbitrary unstructured meshes with local dynamic adaptive mesh refinement using OpenFOAM. arXiv, 1305 3417 v1.
Marić, T., Marschall, H., Bothe, D., 2015. lentFoam – a hybrid level set/front tracking method on unstructured meshes. Comput. Fluids 113, 20–31.
Márquez Damián, S., 2013. An Extended Mixture Model for the Simultaneous Treatment of Short and Long Scale Interfaces PhD Thesis. Universidad Nacional Del Litoral, Argentina.
Ménard, T., Tanguy, S., Berlemont, A., 2007. Coupling level set/VOF/ghost fluid methods: validation and application to 3d simulation of the primary break-up of a liquid jet. Int. J. Multiphase Flow 33, 510–524.
Meredith, K., de Vries, J., Wang, Y., Xin, Y., 2013. A comprehensive model for simulating the interaction of water with solid surfaces in fire suppression environments. Proc. Comb. Inst 34, 2719–2726.
Min, C., 2010. On reinitializing level set functions. J. Comp. Phys. 229, 2764–2772.
OpenFOAM v.2.1.1..
Owen, I., Ryley, D.J., 1985. The flow of thin liquid films around corners. Int. J. Multiphase Flow 11, 51–62.
Pringuey, T, Cant, R.S., 2014. Robust conservative level set method for 3D mixed-element meshes - application to LES of primary liquid-sheet breakup. Commun. Comput. Phys. 16, 403–439.
Puthenveettil, B.A., Senthilkumar, V.K., Hopfinger, E.J., 2013. Motion of drops on inclined surfaces in the inertial regime. J. Fluid Mech. 726, 26–61.
Scardovelli, R., Zaleski, S., 1999. Direct numerical simulation of free-surface and interfacial flow. Annu. Rev. Fluid Mech. 31, 567–603.
Shikhmurzaiev Y., D., 2008. Capillary Flows with Forming Interfaces. Chapman & Hall/CRC.
Šikalo, Š., Wilhelm, H.D., Roisman, I.V., Jakirlić, S., Tropea, C., 2005. Dynamic contact angle of spreading droplets: experiments and simulations. Phys. Fluids 17, 062103.
Sui, Yi., Ding, Hang, Spelt Peter, D.M., 2014. Numerical simulations of flows with moving contact lines. Annu. Rev. Fluid Mech. 46, 97–119.
Sussman, M., Puckett, E.G., 2000. A coupled level set and volume-of-fluid method for computing 3d and axisymmetric incompressible two-phase flows. J. Comp. Phys. 162, 301–337.
Sussman, M., Smereka, P., Osher, S., 1994. A level set approach for computing solutions to incompressible two-phase flow. J. Comp. Phys. 114, 146–159.
Sussman, M., Smith, K.M., Hussaini, Y., Ohta, M., Zhi-Wei, R., 2007. A sharp interface method for incompressible two-phase flows. J. Comp. Phys. 221, 469–505.
Tanner, L.H., 1979. The spreading of silicone oil drops on horizontal surfaces. J. Phys. D: Appl. Phys. 12.
Tryggvason, G., Bunner, B., Esmaeeli, A., Juric, D., Al-Rawahi, N., Tauber, W., Han, J., Nas, S., Jan, Y.-J., 2001. A front-tracking method for the computations of multiphase flow. J. Comp. Phys. 169, 708–759.
Van Leer, B., 1974. Towards the ultimate conservative difference scheme, II. Monotonicity and conservation combined in a second order scheme. J. Comp. Phys. 14, 361–370.
Voinov, O., 1976. Hydrodynamics of wetting. Fluid Dynamics 11, 714–721.
Wang, Z., Yang, J., Koo, B., Stern, F., 2009. A coupled level set and volume-offluid method for sharp interface simulation of plunging breaking waves. Int. J. Multiphase Flow 35 (3), 227–246.
Weller, H., 2008. A New Approach to VOF-based Interface Capturing Methods for Incompressible and Compressible Flows. OpenCFD Ltd. Report TR/HGW/04.
Xiao, F., 2012. Large Eddy Simulation of Liquid Jet Primary Breakup PhD thesis. Loughborough Univ., U.K.
Xiao, F., Dianat, M., McGuirk, J.J., 2013. Large Eddy simulation of liquid-jet primary breakup in air crossflow. AIAA J. 51 (12), 2878–2893.
Xiao, F., Dianat, M., McGuirk, J.J., 2014a. LES of turbulent liquid jet primary breakup in turbulent coaxial air flow. Int. J. Multiphase Flow 60, 103–118.
Xiao, F., Dianat, M., McGuirk, J.J., 2014b. Large Eddy simulation of single drop and liquid jet primary breakup. Atomization and Sprays 24, 281–302.
Yamamoto, T., Okano, Y., Dost, S., 2016. Validation of the S-CLSVOF method with the density-scaled balanced continuum surface force model in multiphase systems coupled with thermocapillary flows. Int. J. Numer. Meth. Fluids doi:10.1002/fld.4267.
Yokoi, K., Vadillo, D., Hinch, J., Hutchings, I., 2009. Numerical studies of the influence of dynamic contact angle on a droplet impacting on a dry surface. Physics of Fluids 21, 072102.
Yokoi, K., 2013. A practical numerical framework for free surface flows based on CLSVOF method, multi-moment methods and density-scaled CSF model: numerical simulations of droplet splashing. J. Comp. Phys. 232, 252–271.